JCTC Journal of Chemical Theory and Computation

pubs.acs.org/JCTC Article

The Good, the Bad, and the Ugly: Pseudopotential Inconsistency Errors in Molecular Applications of Density Functional Theory

Elliot Rossomme, Leonardo A. Cunha, Wanlu Li, Kaixuan Chen, Alexandra R. McIsaac, Teresa Head-Gordon, and Martin Head-Gordon*

Cite This: J. Chem. Theory Comput. 2023, 19, 2827−2841 Read Online

ACCESS | Metrics & More | Article Recommendations | Supporting Information

ABSTRACT: The pseudopotential (PP) approximation is one of the most common techniques in computational chemistry. Despite its long history, the development of custom PPs has not tracked with the explosion of different density functional approximations (DFAs). As a result, the use of PPs with exchange/correlation models for which they were not developed is widespread, although this practice is known to be theoretically unsound. The extent of PP inconsistency errors (PPIEs) associated with this practice has not been systematically explored across the types of energy differences commonly evaluated in chemical applications. We evaluate PPIEs for a number of PPs and DFAs across 196 chemically relevant systems of both transition-metal and main-group elements, as represented by the W4-11, TMC34, and S22 data sets. Near the complete basis set limit, these PPs are found to cleanly approach all-electron (AE) results for noncovalent interactions but introduce root-mean-squared errors (RMSEs) upwards of 15 kcal mol^{-1} into predictions of covalent bond energies for a number of popular DFAs. We achieve significant improvements through the use of empirical atom- and DFA-specific PP corrections, indicating considerable systematicity of the PPIEs. The results of this work have implications for chemical modeling in both molecular contexts and for DFA design, which we discuss.

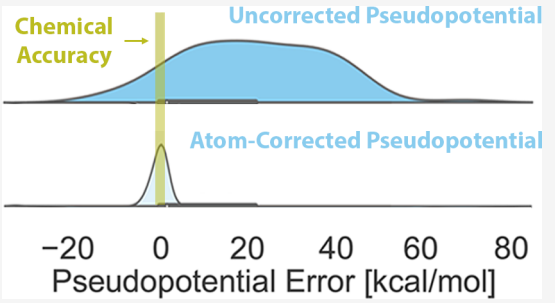

1. INTRODUCTION

Since its inception nearly a century ago,[1] the pseudopotential (PP) approximation has been a widespread approach for enabling molecular and (particularly) condensed matter electronic structure calculations. While PPs initially gained traction for use in solid-state physics,[2−4] their use in chemical applications was not long to follow.[5] In these latter applications, PPs have come to enjoy broad use, and they are routine for the efficient inclusion of electronic relativistic effects[6] and modeling large, complex systems.[7−10] PP development has paced alongside expanding applications, resulting in many options for computational chemists.[6,9,11−15]

Strictly speaking, PPs are developed for use in conjunction with particular methods of electron exchange and correlation.[16−18] For instance, a PBE PP is designed to be used in PBE computations and may not perform well in other contexts.[10,19,20] Nevertheless, it is common to report results obtained with mismatched methods and PPs. While these formally inconsistent protocols are relatively benign in some cases,[9,21−23] they are not theoretically sound and can lead to significant errors.[19,20,23−31] For instance, previous work by some of us identified PP inconsistency errors (PPIEs) as a significant obstacle to accurate modeling of catalysis systems.[20] Others have found that inconsistent PP methods result in significant errors in band gap determinations for solids,[18,19,29] excitation and bond energies in molecules,[19,20,28,31] and other physical parameters.[31]

The importance of PP consistency has been recognized in the solid-state community in recent years. Indeed, the PSEUDODOJO project provides tools to generate plane-wave-compatible PPs for most local density approximation (LDA) and generalized gradient approximation (GGA) density functionals.[32] While development of this project is ongoing, it currently does not provide support for all types of density functionals; furthermore, it is not available for codes that employ Gaussian basis sets. Thus, given the large number of available density functional approximations (DFAs) and the relatively small number of optimized PPs, many computations today must necessarily employ PPs inconsistently. This is particularly true in molecular contexts, where the role of the resulting errors is not well characterized.

Herein, we evaluate the performance of the PP approximation and the extent of PPIEs across a variety of commonly used density functional approximations (DFAs). In this work,

Received: January 20, 2023
Published: May 8, 2023

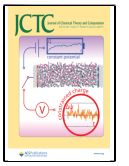

https://doi.org/10.1021/acs.jctc.3c00089
J. Chem. Theory Comput. 2023, 19, 2827−2841

we consider the performance of most major classes of PPs in routine use for chemical applications, as described in Section 1.1. We present all of our computational procedures, including details of benchmark data sets, calculation parameters, and the inclusion of scalar relativistic effects in all-electron computations, in Section 2. Results across all electronic structure methods, PPs, and data sets are discussed in Section 3, and recommendations for future practice are given in Section 4.

1.1. Theory and Structure of Pseudopotentials. At its core, the PP approximation rests on the assumption that only electrons in some defined valence space are relevant to an application of interest.[10] This can be justified by the relatively small polarizability of core electrons, meaning that their orbitals do not vary much in typical chemical processes, though exceptions such as core excitations exist.[33] Ignoring these, core electrons can be removed from the model, replacing the exact Hamiltonian with a simplified operator that possesses eigenvalues and eigenvectors similar to those of the exact system, reducing computational complexity in a number of ways.[9] First, by definition, PPs reduce the number of electrons in a system, decreasing its size. As a corollary of eliminating the core electrons, overall pseudowave functions can be made smoother;[10,19] therefore, smaller basis sets may be adequate,[15] providing clear computational benefits, particularly in plane wave calculations.

Though the separation of core and valence electrons is, strictly speaking, unphysical (electrons are indistinguishable), we can write a model Hamiltonian ($\hat{H}_v$) that describes the physics of this contrived system. Specifically, for N_v valence electrons (coordinates i, j), of an atom a, we have

$$\hat{H}_v = -\frac{1}{2}\sum_{i}^{N_v} \nabla_i^2 + \sum_{i<j}^{N_v} \frac{1}{r_{ij}} + \sum_{i}^{N_v} V_a^{\mathrm{PP}}(r_i) \tag{1}$$

where V_a^{PP} is the atomic pseudpotential.[9] This expression can easily be generalized to a molecular context through the inclusion of additional cores and a classical core−core repulsion term. We will not do this here, and we will drop the a subscript in the following equations. While a number of different formalisms for V^{PP} exist, they generally contain both local (V_{loc}) and nonlocal (V_{nl}) components such that

$$V^{\mathrm{PP}} = V_{\mathrm{loc}} + V_{\mathrm{nl}} \tag{2}$$

The first term on the right-hand side of eq 2 corresponds to the long-range Coulomb potential of the eliminated core electrons and the nucleus they screen. The most straightforward definition of V_{loc} is a perfectly screened Coulomb potential,

$$V_{\mathrm{loc}}(r) = -\frac{Z_{\mathrm{ion}}}{r} \tag{3}$$

where Z_{ion} is obtained as the nuclear charge less the charge of the electrons eliminated by the PP. To improve numerical stability, particularly in plane wave codes, Gaussian smearing is often applied to the nuclear charge, resulting in a modified local potential

$$V_{\mathrm{loc}}(r) = -Z_{\mathrm{ion}}\frac{\mathrm{erf}(r/\sigma)}{r} \tag{4}$$

where σ specifies the width of the Gaussian charge distribution.[10] Other terms may be added to V_{loc} as well depending on the formalism.[14,15]

While V_{loc} captures important aspects of the physics of the eliminated core, it is inadequate for obtaining accurate PP computations.[19] Given the nature of electron exchange, it is unsurprising that the inclusion of nonlocal terms improves the PP performance significantly.[9] A number of different forms for V_{nl} exist, but they generally decompose V^{PP} in terms of angular momentum eigenstates (the spherical harmonics, $Y_{l,m}$) to account for the hierarchy of l shells within the core and to incorporate l-dependent exchange effects.[34] Hence, V_{nl} takes the form of a projector along angular momentum eigenstates scaled by an l-dependent potential, V_l, viz.,

$$V_{\mathrm{nl}} = \sum_{l}^{l_{\max}-1} V_l P_l = \sum_{l}^{l_{\max}-1} \sum_{m=-l}^{l} V_l |lm\rangle\langle lm| \tag{5}$$

Here, $l_{\max}$ is the largest angular momentum represented in the (removed) core orbitals. All valence pseudoorbitals with $l \geq l_{\max} - 1$ experience the same potential $V_{l_{\max}}$ that is usually of similar form to V_l for $l < l_{\max} - 1$.[35] The overall potential V_{nl} can then be written as[6]

$$V_{\mathrm{nl}} = V_{l_{\max}} - \sum_{l}^{l_{\max}-1} (V_l - V_{l_{\max}})P_l \tag{6}$$

where the exact form of V_l changes with the PP.

This framework can be expanded to include the relativistic effects of core electrons, where they are the most important.[6,36,37] Because spin−orbit (SO) coupling lifts addition degeneracies in the angular momentum eigenstates, the projection operators become

$$P_{lj} = \sum_{m} |jlm\rangle\langle jlm| \tag{7}$$

and eq 6 contains an additional sum over total angular momentum quantum number j, affording

$$V_{\mathrm{nl}}^{\mathrm{rel}} = V_{l_{\max},j_{\max}} - \sum_{l}^{l_{\max}-1} \sum_{j=|l-1/2|}^{l+1/2} (V_{lj} - V_{l_{\max},j_{\max}})P_{lj} \tag{8}$$

The effects of SO coupling may be treated in an average way to recover a relativistic PP without an explicit dependence on the j quantum number for each l subspace,[38,39] given by

$$V_l^{\mathrm{avg}}(\mathbf{r}, \mathbf{r}') = \frac{1}{2l+1}[lV_{l-1/2}(\mathbf{r}, \mathbf{r}') + (l+1)V_{l+1/2}(\mathbf{r}, \mathbf{r}')] \tag{9}$$

The form for the SO term can then be derived[40] as the difference between the full relativistic PP and V_l^{avg}. Properties of the projection operators and the angular momentum eigenstates can be exploited to obtain a simplified expression

$$\Delta V_l^{\mathrm{SO}} = \sum_{l=1}^{l_{\max}-1} \frac{\Delta V_l^{\mathrm{rel}}}{2l+1}[lP_{l,l+1/2} - (l+1)P_{l,|l-1/2|}] \tag{10}$$

where the difference potential $\Delta V_l^{\mathrm{rel}}$ corresponds to the relativistic potential between neighboring $Y_{l,m}$ states, i.e.,

$$\Delta V_l^{\mathrm{rel}} = V_{l,l+1/2}^{\mathrm{rel}} - V_{l,|l-1/2|}^{\mathrm{rel}} \tag{11}$$

Alternatively, the SO difference potential may be written in a form that is explicit in the SO interaction,

https://doi.org/10.1021/acs.jctc.3c00089
J. Chem. Theory Comput. 2023, 19, 2827−2841

$$\Delta V_l^{\mathrm{SO}} = \sum_{l=1}^{l_{\max}-1} \frac{2\Delta V_l^{\mathrm{rel}}}{2l+1} P_l(\vec{l}\cdot\vec{s}) P_l \tag{12}$$

though this form was developed primarily for use with configuration interaction (CI) calculations that do not concern the present work.[41]

Though a discussion of common PPs follows shortly, the inclusion of one example here illustrates how PPs are ultimately fit to all-electron results. In perhaps the most conceptually straightforward definition, it is common to expand each semilocal potential V_l in a set, $\{k\}$, of Gaussian-weighted polynomials,[35,42,43] yielding

$$V_l(r_i) = \sum_k B_{lk} r_i^{n_{lk}} e^{-\beta_{lk} r_i^2} \tag{13}$$

where B_{lk}, n_{lk}, and β_{lk} are adjustable parameters.[6,9] Such an expansion may also be applied to the relativistic case, introducing additional parameters C_{ljk}, n_{ljk}, and γ_{ljk} in a similar expansion[9]

$$V_l(r_i) = \sum_k C_{ljk} r_i^{n_{ljk}} e^{-\gamma_{ljk} r_i^2} \tag{14}$$

Where applicable, parametrization of the various coefficients in eqs 13 and 14 (and other expressions for different formalisms) results in PPs that are explicitly fit to results of a particular exchange/correlation method.

1.1.1. Desirable Properties of Pseudopotentials. The ideal PP will reproduce desirable physical properties with high fidelity while lowering the computational cost relative to that of an all-electron procedure. In order to achieve this, many have advocated for PPs that satisfy a variety of (sometimes competing) theoretical criteria.[44−48]

1.1.1.1. Norm Conservation. First, many PPs are designed to be norm-conserving.[44] This amounts to requiring charge densities for real and pseudowave functions to agree outside some core radius r_c. Norm conservation is formally achieved by satisfying the following equations[19,44]

$$\tilde{\psi}_i^{(x)}(r) = \psi_i^{(x)}(r) \quad x = 0, 1, 2; \quad r \geq r_c \tag{15}$$

$$\varepsilon_{\mathrm{PP}} = \varepsilon_{\mathrm{AE}} \tag{16}$$

$$\langle \tilde{\psi}_i | \tilde{\psi}_i \rangle = \langle \psi_i | \psi_i \rangle = 1 \tag{17}$$

$$\frac{\partial}{\partial \varepsilon}\left(\frac{d \ln \tilde{\psi}_i}{dr}\right)\bigg|_{\mathrm{R}} = \frac{\partial}{\partial \varepsilon}\left(\frac{d \ln \psi_i}{dr}\right)\bigg|_{\mathrm{R}} \quad R \geq r_c \tag{18}$$

where ψ_i is an all-electron orbital, $\tilde{\psi}_i$ is a pseudoorbital, (x) superscripts refer to xth derivatives with respect to r, and ε refers to the valence energy eigenvalues. These criteria have been found to result in better-conditioned PPs that perform evenly across chemical environments for DFT computations.[16,44] Strict adherence to norm conservation for HF PPs results in nondecaying tails, and localization schemes are necessary to obtain accurate and well-defined results.[49,50]

1.1.1.2. Shape Consistency. Early work expanded the pseudoorbital $\tilde{\psi}_i$ as a linear combination of the (AE) valence orbital ψ_{v_i} and core orbitals ψ_{c_j}, viz.,

$$\tilde{\psi}_i = C_{v_i}\psi_{v_i} + \sum_j^{N_c} C_{c_j}\psi_{c_j} \tag{19}$$

where C_{v_i} and C_{c_j} are expansion coefficients for virtual and core orbitals, respectively.[3,51] This formalism spuriously stores the valence electron density in the core region,[11] resulting in bond lengths that are too short and potential wells that are too deep.[51] Christiansen et al. proposed a new definition

$$\tilde{\psi}_i = \psi_{v_i} + f_i \tag{20}$$

where f_i is zero for $r \geq r_c$ and is chosen to cancel oscillations in ψ_i for $r < r_c$.[11] This alternate definition corrected the aforementioned core/valence problems and improved the PP performance significantly (*vide infra*). Subsequent shape-consistent PPs were developed to improve the computational efficiency.[52]

1.1.1.3. Energy Consistency. Instead of fitting to orbital properties, some have opted to parametrize PPs to achieve agreement with energetic properties directly,[53] generally emphasizing that this approach focuses exclusively on observables.[54] Despite not being optimized for this outcome, energy-consistent PPs are guaranteed to satisfy eq 18 and thereby achieve some degree of shape consistency.[6,55] Energy-consistent PPs are usually fit to a number of atomic reference states, and this generally results in a strong performance across distinct bonding environments.[6]

1.1.2. Common Classes of Pseudopotentials. Overviews for each of the types of PP used in this study are provided in the following paragraphs, emphasizing the PP structure, development, and performance. Various review articles provided more detailed treatments for the interested reader.[4,6]

1.1.2.1. CRENB Pseudopotentials. The Christiansen−Ross−Ermler−Nash−Bursten (CRENB) pseudopotentials were the first shape-consistent Hartree−Fock pseudopotentials, designed to ensure that radial wave functions of main-group pseudoorbitals closely mirrored all-electron orbitals in the valence space.[11] The form of these potentials is determined by inverting the radial Schrödinger equation and fitting the core region of the pseudoorbital as a polynomial expansion, with the requirement that the magnitude and first three derivatives of the expansion smoothly transition to the exact valence orbital outside the core. This procedure brought about significant improvements for PP predictions of geometric properties and dissociation energies for F_2, Cl_2, and LiCl dimers, where earlier PPs resulted in relative errors of up to 70%.[51,56] These PPs were subsequently extended to include relativistic effects and all elements of the periodic table through Rn, including both large- and small-core variants (CRENBL and CRENBS, respectively).[57−60] Recent work to restructure the radial form of these potentials has resulted in significant improvements in computational cost without affecting the numerical accuracy.[61]

1.1.2.2. Stuttgart Pseudopotentials. In contrast, energy-consistent Stuttgart relativistic PPs are designed only to reproduce observable quantities such as atomic excitation and ionization energies.[54,62] Motivation for this approach came from earlier work showing superb agreement between PP and AE results for dissociation energies for a variety of atoms, ions, and dimers.[12,53,63−67] Furthermore, relaxation of the space consistency constraint accommodates a simpler PP with the following form

$$V_i^{\mathrm{PP}} = -\frac{Z_{\mathrm{ion}}}{r_i} + \sum_{l=0}^{l_{\max}} \sum_k A_{lk} \exp(-\alpha_{lk} r_i^2) P_l \tag{21}$$

https://doi.org/10.1021/acs.jctc.3c00089
J. Chem. Theory Comput. 2023, 19, 2827−2841

where P_l is a projector onto the subspace with angular momentum l and A_{lk} and a_{lk} are parameters that are adjusted to minimize the least-squares error between PP results and all-electron, relativistic HF computations.[53] Generally speaking, fewer Gaussian functions are necessary in SRXC potentials (i.e., k is small), resulting in more efficient implementation.[61,62] Here too, both small-core and large-core (SRSC and SRLC) formulations exist for many elements. Furthermore, the agreement between AE and SRXC radial wave functions in the valence region can be quite good, despite the fact that these PPs are not optimized for this outcome.[54]

1.1.2.3. Karlsruhe Pseudopotentials. The popular Karlsruhe basis sets[68,69] were developed for use with previously published small-core Stuttgart PPs.[12,70−73] Following the convention of the basis set labeling, this PP set is termed def2-ECP. Unlike most PP schemes, core electrons are removed only for the fourth- and fifth-row elements (Rb-Rd); all-electron computations are used for all other elements. It is interesting that basis set convergence for the Karlsruhe series is more rapid for DFT than wave function methods, even though these were parametrized with reference to all-electron HF computations.[69,73]

1.1.2.4. Dual-Space Separable Pseudopotentials. In plane wave contexts, it is advantageous to develop PPs with optimal behavior in both real and reciprocal space. This provided the impetus for Goedecker−Teter−Hutter (GTH) PPs.[14] The GTH local potential is obtained by smearing the screened nuclear charge (eq 4) and adding this to a Gaussian-weighted polynomial, and the nonlocal potential is given by

$$V_{\mathrm{nl}}(\mathbf{r}) = \sum_{l,m,i,j} Y_{l,m}(\hat{\mathbf{r}})\, p_{l,i}(r)\, h_{i,j} p_{l,j}(r')\, Y_{l,m}(\hat{\mathbf{r}}') \tag{22}$$

where $Y_{l,m}$ represents the spherical harmonics, $p_{l,i}$ represents the Gaussian radial projector for angular momentum l, and $h_{i,j}$ represents the expansion coefficients for the projectors. Though somewhat obscured by the formalism, these potentials and their Fourier transforms both consist of Gaussian-weighted polynomials, which are advantageous for computational and physical reasons.[14] The parameters in GTH PPs are least-squares optimized to maximize agreement with all-electron charge density and select (occupied and virtual) orbital energy eigenvalues, and this was completed separately for the LDA and BLYP functionals in the original publication. The inclusion of relativistic effects results in Hartwigsen−Goedecker−Hutter (HGH) potentials, which have been optimized with the LDA functional for all elements through Rn.[15] Additional parametrizations have been reported for BLYP,[17] BP,[17] PBE,[17,74,75] B97M-rV,[20] and ωB97X-V[20] density functionals.

1.1.2.5. Projector Augmented Waves. The projector augmented wave (PAW) approach[13] is conceptually similar to the PPs discussed above in that it creates a partition between core and valence electrons. Here, the pseudototal wave function $\tilde{\psi}$ is related to the AE wave function ψ through a linear transformation such that

$$|\psi\rangle = |\tilde{\psi}\rangle + \sum_i (|\varphi_i\rangle - |\tilde{\varphi}_i\rangle)\langle \tilde{p}_i|\tilde{\psi}\rangle \tag{23}$$

where φ_i and $\tilde{\varphi}_i$ are the partial waves and pseudopartial waves, respectively, and $\tilde{p}_i$ is a projector onto the space of $\tilde{\varphi}_i$.[13,76] As in the case of PPs described above, the index i specifies an atomic center and angular momentum quantum numbers (l, m). The basis of $\tilde{\varphi}_i$ functions is complete such that the expansion in eq 23 is exact in the infinite limit.[13] In practice, only one or two partial waves $\tilde{\varphi}_i$ are used for each set of angular momentum quantum numbers.[10] These projectors are localized to a predefined core region,[13] and the size of this region impacts the accuracy of a computation considerably.[10] As above, the partial wave expansion is fit to results from a particular AE method, and a number of parametrizations have been reported.[77,78]

1.2. Pseudopotential (In)consistency. Regardless of the details in form, each of the preceding PPs undergoes some fit procedure to achieve agreement with a particular set of all-electron computations. As a result, a PP computation is only theoretically sound if it employs the same methods of electron exchange and correlation as were used to paramaterize the PP.[19,21] Indeed, much of the groundbreaking work on PPs for chemical applications anticipated reparametrization with more accurate correlation treatments in the future.[14,16,24] This has not, however, always been the case, and errors associated with the "inconsistent" use of PPs are well-documented.

It is somewhat common to acknowledge the lack of theoretical footing for inconsistent PP use but advocate this practice anyway on the basis of empirical results.[9,21−23] These studies generally compare geometries and energetic properties for a few (<10) small systems to all-electron results and show that errors incurred by PPs are smaller than those due to other approximations, such as basis set truncation and inexact correlation treatments. To be fair, there are certainly cases in which pseudopotential inconsistency errors (PPIEs) are quite small. For instance, ref 23 provides mean absolute errors (MAEs) due to the use of HF potentials in DFT computations across six small transition-metal complexes; these are 0.4 and 0.6 kcal mol^{-1} for S-VWN and B-LYP density functionals, respectively. However, this same paper reports errors of −7.4 and −13.2 kcal mol^{-1} for binding energies of TiF_4 and $Ni(CO)_4$ when the S-VWN potential is used with B-LYP and presents these results as tolerable. Similar patterns are present in the other cited sources, where good (even great) performance for a small number of systems is extrapolated to justify inconsistent PP use broadly despite the fact that performance is not uniform.

Indeed, a number of other studies have reached the opposite conclusion, finding PP reparameterization is necessary to achieve high fidelity with AE computations.[15,18−20,26] To take a recent instance, the use of a PBE0 potential in lieu of a PBE potential reduced mean absolute relative PP errors from 8 to 4.5% in comparison to all-electron results.[19] This finding is consistent with other work that indicates that methods employing exact exchange (HF, hybrid DFT) require PPs that incorporate these effects.[18,26] Likewise, results from ref 28 indicate that the use of the SRSC potential (fit to HF results[54]) in DFT computations results in inconsistency MAEs ranging from about 1 to 15 kcal mol^{-1} for lanthanide complexes, depending on the density functional. Additionally, previous work from some of us found that use of the GTH-PBE[14,17] in B97M-rV and ωB97X-V computations incurred mean absolute PPIEs of 5.1 and 4.6 kcal mol^{-1} for binding energies of the first-row transition-metal monocarbonyls.[20] Parameterization of new GTH potentials for these functionals reduced these MAEs to 3.5 and 2.4 kcal mol^{-1}, respectively.

Despite the long-time recognition of theoretical and practical limitations of inconsistent PP use, systematic

https://doi.org/10.1021/acs.jctc.3c00089
J. Chem. Theory Comput. 2023, 19, 2827−2841

Table 1. Core Size for Each of the Five Pseudopotentials Included in This Study across All Relevant Elements[a]

Elements	def2-ECP[b]	fit-CRENBL[c]	SRLC[d]	GTH[e]	PAW[f]
B−F	–	[He]	[He]	[He]	[He]
Al−Cl	–	[Ne]	[Ne]	[Ne]	[Ne]
Sc−V	–	[Ne]	[Ar]	[Ne]	[Ne]
Cr−Mn	–	[Ne]	[Ar]	[Ne]	[Ne] + 3*s*
Fe	–	[Ne]	[Ar]	[Ne]	[Ar]
Cu−Zn	–	[Ne]	[Ar]	[Ar]	[Ar]
Y−Mo	[Ar] + 3*d*	[Ar] + 3*d*	–	[Ar] + 3*d*	[Ar] + 3*d*
Tc−Rh	[Ar] + 3*d*	[Ar] + 3*d*	–	[Ar] + 3*d*	[Ar] + 3*d* + 4*s*
Pd	[Ar] + 3*d*	[Ar] + 3*d*	–	[Ar] + 3*d*	[Kr]
Ag−Cd	[Ar] + 3*d*	[Ar] + 3*d*	–	[Kr]	[Kr]
Hf−Ta	[Kr] + 4*d* + 4*f*	[Kr] + 4*d* + 4*f*	–	[Kr] + 4*d* + 4*f*	[Kr] + 4*d* + 4*f* + 5*s*
W	[Kr] + 4*d* + 4*f*	[Kr] + 4*d* + 4*f*	–	[Kr] + 4*d* + 4*f*	[Kr] + 4*d* + 4*f*
Re−Pt	[Kr] + 4*d* + 4*f*	[Kr] + 4*d* + 4*f*	–	[Kr] + 4*d* + 4*f*	[Xe] + 4*f*
Au−Hg	[Kr] + 4*d* + 4*f*	[Kr] + 4*d* + 4*f*	–	[Xe] + 4*f*	[Xe] + 4*f*

[a]Highlighted blocks correspond to successive rows of the periodic table. [b]Ref 81. [c]Refs 57−61. [d]Ref 62. [e]Refs 14 and 15. [f]Ref 76.

Table 2. Basis Set and Pseudopotential Combinations Used for Various Computations in This Work[a]

All-Electron	S22	W4-11	TMC34
BSIE ref.	def2-QZVPPD	def2-QZVPPD	def2-QZVPPD[b]
PP ref.	def2-QZVPPD	def2-QZVPPD	TZVPPall (+X2C)
Truncated basis	def2-TZVPPD	def2-TZVPP	def2-TZVPP
Pseudopotential	**S22**	**W4-11**	**TMC34**
fit-CRENBL	def2-QZVPPD	def2-QZVPPD	def2-TZVPP
SRLC	def2-QZVPPD	def2-QZVPPD	–
GTH-PBE	–	TZV2P	TZV2P
PAW-PBE	–	1000 eV	1000 eV

[a]Citations for each basis set are found in the text. [b]Results obtained only for the TMD10 subset.

exploration of this issue is absent from the literature. In solid state contexts, commendable work from Borlido et al. examined the inconsistent use of PAW potentials for the determination of band gaps for 473 materials with a variety of common density functionals.[29] These researchers found that the inconsistent use of PPs increased errors at least 3-fold relative to consistent computations but that these generally incurred MAEs of around 0.1 eV, which are argued to be tolerable in solid-state contexts. Even so, errors for individual systems yawned to multiple eV in some instances, and problematic cases could not be identified in any predictable way.[29]

Studies of similar scope for PP consistency errors in properties of chemical interest have not been reported, even as the use of PPs in these contexts expands, particularly in *ab initio* molecular dynamics where PPs may be applied to all atoms[7,8,79,80] As discussed above, select results in this domain are mixed, making broad recommendations for practice difficult. In the present work, we address this by evaluating PPIEs incurred for HF and various forms of the density functional approximation (DFA), including local density approximations (LDAs), generalized gradient approximations (GGAs), meta-GGAs, and hybrids. We evaluate these errors for fit-CRENBL, SRLC, def2-ECP, GTH-PBE, and PAW-PBE potentials across a diverse set of 196 benchmark energies, including atomization energies for main-group elements, nonbonded interactions, and both barrier heights and reaction energies for transition-metal dimers and organometallic complexes. These DFAs, PPs, and data sets are described in Section 2, and our results are presented in Section 3.

2. METHODS

Pseudopotential (PP) errors, including inconsistency errors, were determined with reference to all-electron results across a variety of exchange and correlation methods. We report these errors for three diverse benchmark data sets, described in Section 2.1. In order to include a breadth of the PP classes described above, we employed a number of different electronic structure codes. Essential aspects of each of these computations can be found in Section 2.2. For systems involving transition metals, we include scalar relativistic effects through the exact two-component (X2C) framework,[33] which we briefly describe in Section 2.3.

2.1. Benchmark Data Sets. Performance was evaluated across a diverse collection of benchmark data sets representing the broad range of interactions relevant to complex chemical systems. Nonbonded interactions were represented by the S22 set of noncovalent dimers, which encompass a range of intermolecular forces, including hydrogen bonds.[82] The W4-11 set of 140 total atomization energies for small first- and second-row molecules and radicals was used to evaluate the performance for main-group (MG) thermochemistry.[83] Finally, PP performance for transition-metal (TM) chemistry was evaluated using the TMC34 set,[84] which is composed of three subsets: (a) the TMD10 set of first-row TM dimers with MG elements,[85] (b) the MOR13 set of metal−organic reaction energies for TM complexes,[86] and (c) the TMB11 set of TM barrier heights for reactions in second- and third-row TM complexes.[87−91] Further details about the composition of each data set can be found in Section S3.2.

For all results presented in the main text, published benchmark geometries were used for computations. The

https://doi.org/10.1021/acs.jctc.3c00089
J. Chem. Theory Comput. 2023, 19, 2827−2841

impact of geometry optimization on benchmark energies is explored for select systems and methods in Section S2.3, where it is found to be negligible.

2.2. Computational Details. Pseudopotential (PP) errors were evaluated in comparison to all-electron (AE) computations across a variety of PPs, including def2-ECP,[81] fit-CRENBL,[57−61] SRLC,[62,92] PAW-PBE,[13,76] and GTH-PBE.[14,15,17] Core sizes for each of these PPs are found in Table 1, and further descriptions are in Section 1.1. We study the use of these PPs in conjunction with different electron exchange and correlation methods, including Hartree−Fock (HF) theory[93−96] and five density functional approximations (DFAs): LDA,[97] PBE,[98] SCAN,[99] B97M-rV,[100,101] and ωB97X-V.[102] For computations involving transition metals, scalar relativistic effects were included through the X2C procedure[33] (Section 2.3).

Computations for all-electron results, as well as the def2-ECP, fit-CRENBL, and SRLC PPs, were obtained using the Q-Chem computational chemistry package.[103] These computations employed one of the def2-TZVPP, def2-TZVPPD, or def2-QZVPPD basis sets,[68,69,104] as indicated in Table 2 and the discussion below. For select fit-CRENBL and SRLC computations, additional results were obtained using the native basis sets for these potentials[57,62] augmented with polarization functions from the 6-311(2df,2dp) set.[105,106] Unrestricted reference states were employed, and stability analysis was used to ensure that minimum-energy states were obtained. Fine (99,590) Lebedev integration grids were used to evaluate integrals of the exchange-correlation (XC) functional.[107,108] Energy convergence thresholds of at most 1×10^{-8} a.u. were used to terminate self-consistent field (SCF) iterations, though more stringent convergences of 1×10^{-10} a.u. were obtained in the majority of cases. In troublesome systems, explicit excitations into the valence space resulted in lower-energy solutions; this procedure was used as necessary to ensure that energy comparisons relied on the same electronic state.

Results for PBE and B97M-rV computations with Goedecker−Teter−Hutter (GTH) potentials[14,15] optimized for PBE[17] and B97M-rV[20] were obtained using the CP2K code[109−111] in combination with the molecular optimized (MOLOPT) TZV2P basis set.[112] Kohn−Sham orbitals were optimized using the orbital transformation method[113] for molecules or using the traditional diagonalization approach for metal atoms. Computations were performed using a box size of 20 Å × 20 Å × 20 Å, and the energy cutoff was set at 800 Ry for the calculation of the electrostatic energy terms. SCF iterations were taken to be converged when energy changes were smaller than 1×10^{-6} a.u.

Finally, VASP[77,114] was used for PAW-PBE results obtained with the plane wave (PW) basis set cutoffs indicated in Table 2. All calculations were performed at the gamma point with Gaussian smearing using a width of 0.03 eV. Calculations were performed with 12 Å of vacuum between periodic images. For charged systems, we include monopole and dipole corrections to the energy to avoid spurious interactions between charged periodic replicas. Nonspherical contributions to the gradient correction inside the PAW spheres were included, as was an additional support grid for the augmentation charges. Symmetry was not used in any of these computations. The energy convergence criterion was 2.72114×10^{-9} eV (1×10^{-10} a.u.) for SCAN and PBE functionals and 2.72114×10^{-8} eV (1×10^{-9} a.u.) for HF and B97M-rV functionals, with rare exceptions for a few systems where convergence proved challenging. Basis set convergence studies suggest that basis set errors are <1 kcal mol^{-1} for individual molecules and <0.5 kcal mol^{-1} for all reaction energies, with most systems exhibiting errors lower than those upper bounds.

Throughout this study, PP performance is evaluated in reference to all-electron basis set incompleteness errors (BSIEs), as suggested by other authors.[14] In all cases, energies obtained with the def2-QZVPPD basis set were taken as good approximations to the complete basis set (CBS) limit.[69,104] In a majority of cases, the BSIE associated with the use of the def2-TZVPP set was determined as sets of this quality are generally used in production computations.[69] The def2-TZVPPD set was used, however, for computations on the S22 set, as diffuse functions are known to be important for accurate modeling of noncovalent interactions.[115,116] We do not report BSIEs for the TMB11 and MOR13 subsets of TMC34, as def2-QZVPPD computations for these systems are intractable.

2.3. Relativistic Effects for TMC34 Benchmarks. All-electron scalar (i.e., spin-free) relativistic calculations were performed within the exact two-component (X2C) framework.[117] The X2C model transforms the one-electron Hamiltonian by effectively incorporating information from the solutions of the four-component, one-electron Dirac Hamiltonian.[118−120] Our implementation of X2C has been previously used to study K-edge core spectroscopy of third-period main-group elements and first-row transition metals,[33] where scalar relativistic effects are bound to play a major role. A possible limitation of our relativistic treatment concerns the handling of two-particle interelectronic interactions. Besides being described by a purely Coulombic potential, these terms are left unaltered within the simple X2C formalism. For core spectroscopy of transition metals, a lack of such effects, known as picture-change effects,[119] can lead to large errors in predicting excitation energy,[33] but their effect should be minor for valence electrons in first-row transition metals and our X2C approach should be adequate for these systems.[121] The same convergence criteria and DFT quadrature grids used in the PP calculations were employed for the all-electron X2C counterparts. For the X2C calculations, the decontracted x2c-TZVPPall basis set[122] was used for all elements. This basis set was specifically designed to be consistent with the def2 family of basis sets and provides all-electron support for heavy elements whose cores are usually replaced by PPs. Therefore, our all-electron X2C results allow for a straightforward assessment of PP errors for the transition-metal complexes in this work.

3. RESULTS AND DISCUSSION

We assess the performance of PPs across a wide range of benchmark data sets that encapsulate the types of interactions relevant to complicated multiscale modeling problems, as described in Section 2.1. PP errors are highly heterogeneous across this wide array of systems, prohibiting uniform recommendations for the use of PPs in modeling systems of interest. Throughout this section, we discuss these errors in reference to the magnitude of basis set incompleteness errors (BSIEs) for each system type, which are explored in Section 3.1. We then present results for systems in order of increasing PP errors in Sections 3.2−3.4. We summarize results for all systems in Section 4, and we conclude with recommendations for future work and practice in Section 4.

https://doi.org/10.1021/acs.jctc.3c00089
J. Chem. Theory Comput. 2023, 19, 2827−2841

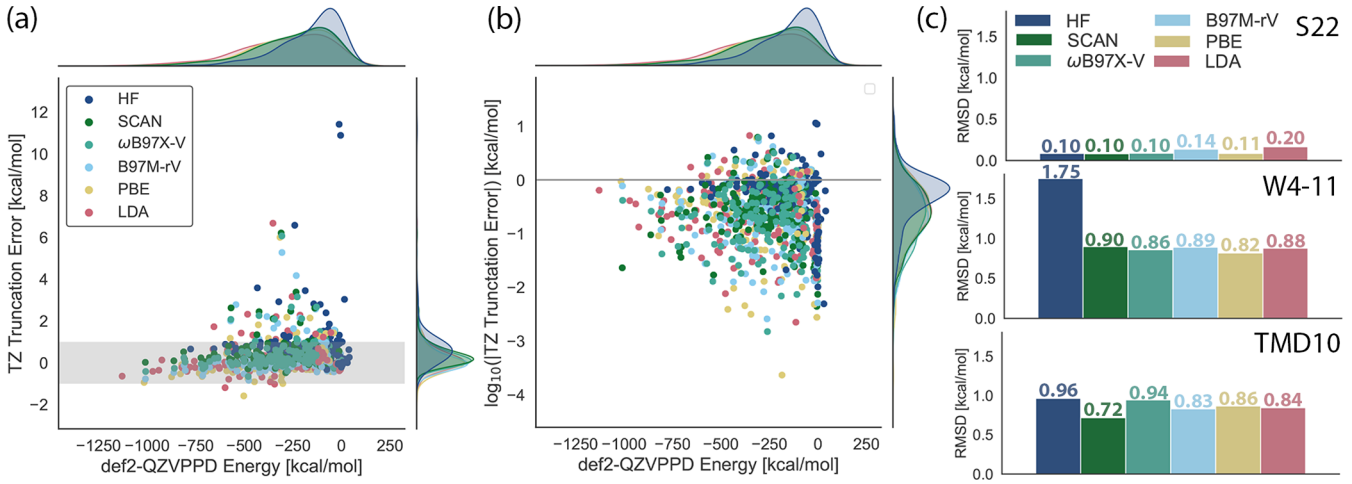

Figure 1. Basis set incompleteness error (BSIE) for all-electron def2-TZVPP results is within the chemical accuracy for most systems: (a) BSIE relative to interaction energy indicates small errors across system size and (b) the base-10 logarithm of the magnitude of BSIE shows that most errors are in the 0.1−1 kcal mol^{-1} range. Chemical accuracy is achieved by points within the gray band in panel (a) and below the gray line in panel (b). (c) Root-mean-squared BSIE satisfies chemical accuracy across methods for the S22, W4-11, and TMD10 data sets, except HF for W4-11, where large errors for FOO and ClOO dominate. Omission of these species lowers the HF RMSE to 1.0 kcal mol^{-1}.

3.1. Scale of the Basis Set Incompleteness Error. The importance of pseudopotential inconsistency errors (PPIEs) in a given calculation should be measured against the scale of other errors in the methodology. It is commonly argued that PPIEs are smaller than basis set incompleteness errors (BSIEs)[14] and/or density functional errors (DFEs);[9,14,23] therefore, PPIEs may be safely ignored. Previous studies have benchmarked DFEs across a range of interactions (cf. Mardirossian and Head-Gordon[123] and citations therein), and we do not repeat this work here. We do, however, report BSIEs across the present data sets and for each of the present DFAs as a reference point for a later discussion of PP errors in these same systems.

Across all of the present systems, def2-TZVPP BSIEs are generally within the bounds of chemical accuracy (<1 kcal mol^{-1}), regardless of the density functional and the system (Figure 1(a)). The logarithm of these BSIEs (Figure 1(b)) provides a fuller picture of these data, indicating that a majority of errors fall within the 0.1−1 kcal mol^{-1} range, although even higher accuracy is achieved for many systems. The slightly positive slope of the data in Figure 1(a) indicates that BSIEs vary only slowly with the interaction size, such that chemical accuracy in the BSIEs is obtained even for systems with very large transformation energies. The logarithm plot (Figure 1(b)) highlights this structure even more clearly, as seen in the slope of the lower edge of accuracy as we vary the system size.

Summary statistics for BSIEs in these systems are also encouraging across each data set, although, as is well known, performance varies considerably from one type of energy difference (and thus one kind of data set) to another (Figure 1(c)). Due to favorable error cancellation, BSIEs are generally small for the nonbonded interactions in the S22 set, with RMS errors of ≲0.2 kcal mol^{-1} for all density functionals. BSIEs are statistically larger for the W4-11 and TMD10 sets, which contain total atomization energies for small main-group molecules and first-row transition-metal dimers, respectively. Across these results, only HF for W4-11 fails to achieve chemical accuracy in the BSIEs, and poor performance for two species (FOO and ClOO) dominates this error. Omission of these entries results in an adjusted RMS error of 1.0 kcal mol^{-1}, still slightly larger than BSIEs for the DFAs. In general, HF energies converge more slowly than DFT energies with the Karlsruhe basis sets, so this is unsurprising.[69,73]

For present purposes, these results define what we consider a tolerable PP error (i.e., one that is smaller than the BSIEs in similar systems). In what follows, we evaluate PP errors for these systems using the BSIE benchmark in conjunction with references to previous results for DFA performance. As seen for the BSIEs, pseudopotential performance is also expected to vary depending upon how well errors cancel out in evaluating energy differences. We shall see below that PP errors range from fractions to tens of kcal mol^{-1}.

3.2. The Good: Barrier Heights and Nonbonded Interactions. The systems in the S22 set were used in order to assess the validity of common pseudopotential approximations in the context of nonbonded interactions. The benchmarks in this set correspond to the dimerization energy of organic monomers, with computed interaction energies ranging from −0.5 to 21 kcal mol^{-1}.[82] Pseudopotential errors were evaluated relative to all-electron def2-QZVPPD calculations for the fit-CRENBL and SRLC potentials on the same basis set.

As seen in Figure 2, PP errors for fit-CRENBL are within the limits of chemical accuracy for all systems in S22 across all DFAs in this study. These deviations are size-extensive in the magnitude of the interaction, as demonstrated by the clear linearity in the errors. This behavior also characterizes the SRLC pseudopotential error for these systems (Figure S1), with average relative errors of about 1−3% for the fit-CRENBL PP and the methods and systems in Figure 2. The largest absolute errors therefore occur in systems with the highest dimerization energies, here, the formic acid dimer, the formamide dimer, and the uracil dimer, each of which possesses two hydrogen bonds. Still, even the largest absolute error of −0.66 kcal mol^{-1} (formic acid dimer, ωB97X-V) is only 3% of the interaction energy, tolerably small for most purposes.

In addition to being small in absolute terms, fit-CRENBL and SRLC errors are smaller than BSIEs for 67 and 59% of the S22 systems, respectively. Given the size of both types of

https://doi.org/10.1021/acs.jctc.3c00089
J. Chem. Theory Comput. 2023, 19, 2827−2841

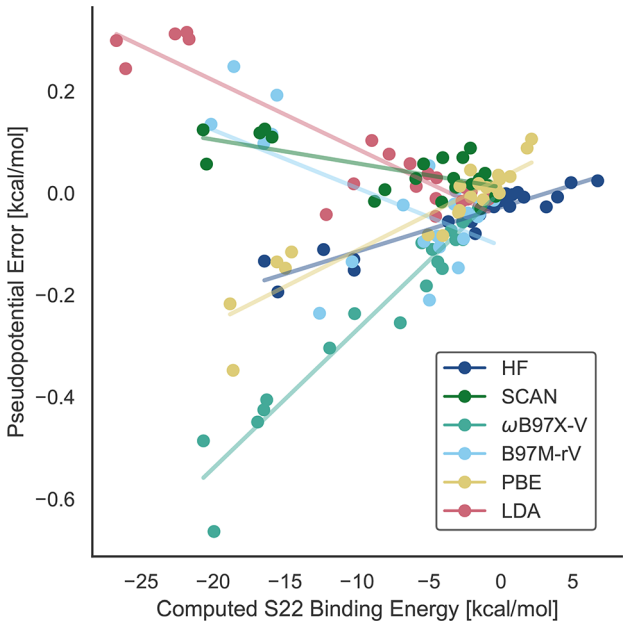

Figure 2. Pseudopotential errors (kcal mol^{-1}) for the S22 data set of intermolecular interactions versus the value of the interaction energy. The errors are defined as deviations between fit-CRENBL/def2-QZVPPD PP calculations and all-electron calculations for each of the six DFAs listed. Errors for all data points are within the chemical accuracy threshold of 1 kcal mol^{-1} and vary linearly with the size of the interaction. Similar results were obtained for the SRLC potential (Figure S1).

errors, failures in the DFA correlation scheme will tend to dictate overall model performance for nonbonded interactions. While these results suggest a small degree of caution in systems with extremely strong intermolecular forces, such as those with multiple hydrogen bonds, they lend general support to the use of the pseudopotential approximation, even with inconsistent application, in nonbonded contexts.

Barrier heights for the transition-metal complex reactions of the TMB11 set also generally exhibited small PP errors (Figure 3). Still, even here, differences in the quality of various PPs emerges. The def2-ECP exhibits the strongest performance and transferability of all considered PPs, with RMSEs of around 0.5 kcal mol^{-1} for all of the DFAs. In part this is because the def2-ECP is more conservative than the other PPs considered here: def2-ECP is all-electron until the second-row transition metals (cf. Table 1). The barrier for Mo-catalyzed splitting of a sulfonyl bond reaction represents a clear and single outlier for the HF/def2-ECP combination with an error of 9.8 kcal mol^{-1}. If this point is omitted, then HF/def2-ECP exhibits the smallest RMSE of all functional/method combinations for the TMB set (0.26 kcal mol^{-1}, down from 2.91 kcal mol^{-1}; see Tables S13 and S16). The GTH-PBE performs similarly well for PBE computations (RMSE = 0.45 kcal mol^{-1}) and exhibits only a small inconsistency error, resulting in a 0.77 kcal mol^{-1} RMSE upon removal of the same sulfonyl splitting reaction barrier discussed above, which is problematic here as well.

TMB 11 results for the PAW-PBE potential as implemented in VASP are more mixed. If charged systems are omitted, then PP errors are in line with the values discussed in the preceding paragraph, with RMSEs of 0.55 and 0.60 kcal mol^{-1} for the PBE and SCAN functionals, respectively. Barrier heights for charged systems are abysmal (Tables S17 and S18), but this represents a known challenge for periodic codes[124,125] and is not an indictment of the PAW-PBE potential. Finally, of the results for the TMB11 set, the fit-CRENBL potential exhibits the worst performance, with DFA-dependent RMS PP errors of 0.8−1.2 kcal mol^{-1}. Once again, Mo-catalyzed sulfonyl splitting exhibits the worst performance for most DFAs, and its omission brings the overall statistics for fit-CRENBL results within chemical accuracy.

Direct comparison to BSIEs cannot be made for the TMB11 systems as many of these reaction complexes are large enough to prohibit near-CBS treatment with the def2-QZVPPD basis. Still, once pathological cases are removed, chemical accuracy is achieved in the majority of cases for all of the DFA/PP combinations considered here. The performance of PPs on transition-metal reaction barrier heights and overall energies for nonbonded interactions are similarly strong, and the present results lend support for even inconsistent use of PPs in such applications.

3.3. The Bad: Transition-Metal Reaction Energies.

Pseudopotential performance degrades upon moving from transition-metal barrier heights to overall reaction energies for similar systems. Within this category, we include the thermodynamics for the MOR13 TM complex reactions and the dimerization energies of TMD10. The latter benchmark set is particularly well-suited for differentiating between different PPs, as their performance varies greatly here.

As before, the def2-ECP and PAW-PBE potentials perform well for the MOR13 reaction energies (Figure 3). DFA/def2-ECP RMSEs hover around chemical accuracy, ranging from 0.9 kcal mol^{-1} for B97M-rV to 1.2 kcal mol^{-1} for SCAN. As in TMB11 above, the HF/def2-ECP error is dominated by a single outlier (Pd-catalyzed splitting of C_2H_6), and the omission of this point brings the RMSE for this methodology to 1.0 kcal mol^{-1} and does not change the other def2-ECP results significantly. RMSEs for PAW-PBE are similar in overall magnitude for MOR13, at 1.2 and 1.0 kcal mol^{-1} for the PBE and SCAN functionals, respectively. Perhaps more than any other result in this study, this demonstrates very good transferability of the PAW-PBE potential as the overall error for SCAN is actually less than that of its native PBE. Additionally, each of the def2-ECP and PAW-PBE potentials is able to consistently capture the scalar relativistic effects associated with these systems as approximated by our X2C calculations.

Neither the GTH-PBE nor the fit-CRENBL potentials provide results as reliable as those for def2-ECP or PAW-PBE for the MOR13 reactions. RMS PP errors for fit-CRENBL span 2.0−3.7 kcal mol^{-1} depending on the method, and one cannot clearly attribute these discrepancies to any single outlier (Figure 3(b)). Indeed, removal of the largest-error species does not significantly improve the statistical picture for fit-CRENBL across any of the correlation methods. Similar comments can be made for GTH-PBE (Figure 3(c)), where the errors for PBE and B97M-rV are 1.9 and 2.8 kcal mol^{-1}, respectively. The increase in error magnitudes from PBE to B97M-rV provides a first indication of the sensitivity of GTH potentials to inconsistency errors, as noted elsewhere.[14,15,17,20] Still, even when used in conjunction with its parent PBE functional, this GTH potential exhibits errors outside of chemical accuracy in all but four of the MOR13 systems. Unlike the treatment of nonbonded interactions and barrier heights, where the performance was relatively good for all PPs assessed, the MOR13 subset discriminates between the PPs

https://doi.org/10.1021/acs.jctc.3c00089
J. Chem. Theory Comput. 2023, 19, 2827−2841

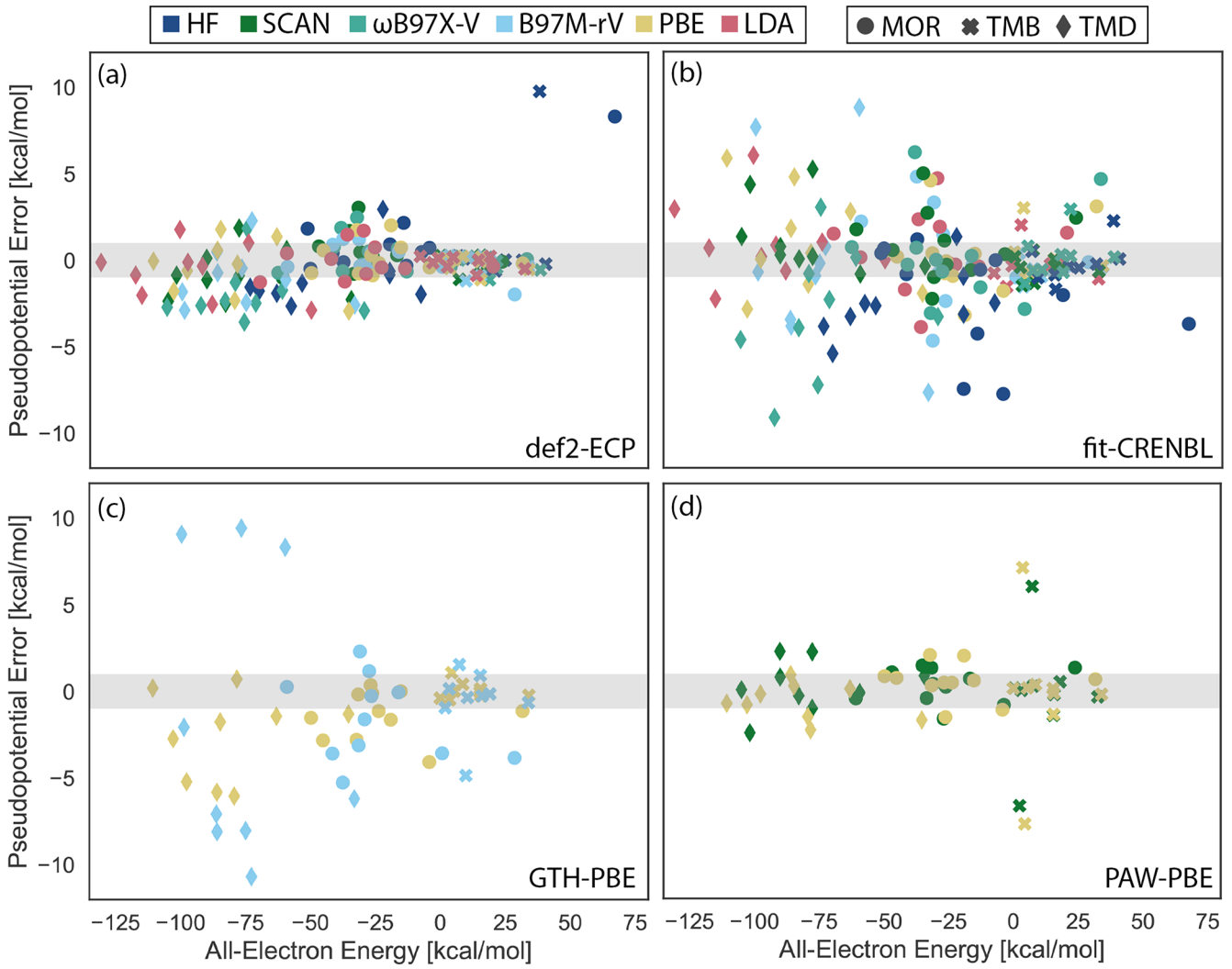

Figure 3. Pseudopotential errors (kcal/mol) for (a) def2-ECP, (b) fit-CRENBL, (c) GTH-PBE, and (d) PAW-PBE for the TMC34 data set of transition metals containing energy changes. TMC34 contains three subsets: barrier heights (TMB; crosses), reaction energies (MOR; circles) and dimer bond strengths (TMD; diamonds). Errors generally increase from TMB to MOR to TMD. Gray bands correspond to a chemical accuracy of ±1 kcal mol^{-1}. Outliers and other aspects of the data are discussed in the text.

considered here, with fit-CRENBL and GTH-PBE exhibiting consistently larger errors than def2-ECP and PAW-PBE.

Discrepancies in PP performance become larger in moving to the TMD10 set of dimerization energies for first-row TM−X complexes, where X is the main-group element. The best results are obtained with PAW-PBE, where PP RMSEs are 1.2 and 1.4 kcal mol^{-1}, respectively, for PBE and SCAN (Figure 3(d)). While included in Figure 3(a), the TMD10 performance is a poor metric for def2-ECP, as this potential is all-electron for the first-row TM series. Thus, def2-ECP errors are largely associated with the neglect of relativistic effects rather than PP success or failure (Section S3.1). Still, RMSEs ranging from 1.6 to 2.5 kcal mol^{-1} for def2-ECP indicate that relativistic effects can be significant even in these systems.

GTH-PBE and fit-CRENBL errors are troubling in these systems. For the latter, RMSEs range from 2.3 kcal mol^{-1} for SCAN to 5.0 kcal mol^{-1} for B97M-rV, and a number of individual fit-CRENBL TMD10 predictions err by over 5 kcal mol^{-1} for each of the tested DFAs. For GTH-PBE, a 3.5 kcal mol^{-1} RMSE for the PBE functional indicates an apparent inadequacy of the GTH procedure, resulting in errors of up to 6 kcal mol^{-1} (for MnBr), affording an RMSE of 3.5 kcal mol^{-1}. Inconsistency errors further plague B97M-rV/GTH-PBE computations, where the smallest PP error is −2 kcal mol^{-1}, and over half of these TMD10 errors are in excess of 8 kcal mol^{-1}. Refitting GTH potentials for each density functional is therefore necessary but by no means sufficient for obtaining high-fidelity results relative to AE computations.

The prediction of dimerization energies between TM and MG atoms therefore represents a challenging problem for PPs, and differences in the performance between PAW and GTH/fit-CRENBL are notable. These differences are consistent with previous findings in solid-state contexts, where the PAW performance was markedly better than for other classes of PPs.[126] Thus, while PPs introduce few errors for barrier heights of TM complexes and relatively small errors for MOR13 reaction energies, atomization energies present significant challenges for some of the most common types of PPs.

3.4. The Ugly: Main-Group Bond Breaking. Pseudopotential errors in dimerization energies for TMD10 portend further trouble for the evaluation of main-group atomization energies such as those of the W4-11 set.[83] Errors for these systems turn out to exhibit an extremely strong dependence on

https://doi.org/10.1021/acs.jctc.3c00089
J. Chem. Theory Comput. 2023, 19, 2827−2841

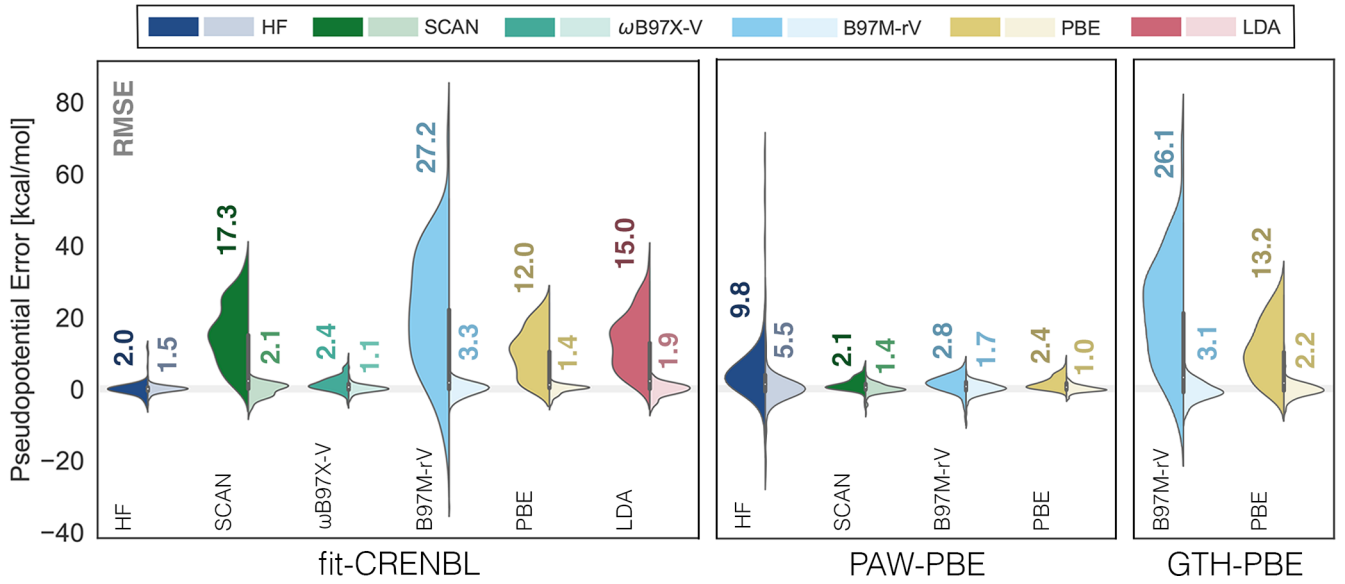

Figure 4. Errors (kcal/mol) in the W4-11 total atomization energies relative to all-electron def2-QZVPPD results. PP errors for each methodology are indicated to the left side of each violin. Inclusion of element-specific atomic corrections significantly improved the performance in all cases (right violins), indicating a large degree in the systematic PP error. Violins are decorated with root-mean-square pseudopotential errors (RMSEs).

the density functional with startling error distributions in some cases (Figure 4).

Once again, out-of-the-box treatments using the PAW-PBE PP provide the most consistently reliable treatment for these systems, with RMSEs of 2.1−2.8 kcal mol^{-1} for the SCAN, PBE, and B97M-rV DFAs. The greatest range of performance for the W4-11 atomization energies is found in fit-CRENBL, where PP RMSEs for HF and ωB97X-V are 2.0 and 2.4 kcal mol^{-1}. Meanwhile, fit-CRENBL errors are unacceptably large for the other four DFAs (Figure 4). For SCAN, B97M-rV, and LDA, PP errors are in excess of 1 kcal mol^{-1} for over 95% of the W4-11 systems. Furthermore, PP errors are larger than def2-TZVPP BSIEs in at least 97% of systems for each of these three DFAs as well as PBE. Errors of this magnitude persist for fit-CRENBL computations even when the native basis set is used (Section S2 and Table S8). For B97M-rV, where errors are the largest, we also demonstrate that these cannot be improved by using method-optimized geometries (Section S2.3). Hence, the general assumption that PP errors are small relative to other computational approximations[9,15,23] clearly does not hold here. The difference with ωB97X-V and HF, where about 45 and 60% of energies are within the chemical accuracy of the AE results, is striking, potentially pointing to the importance of exact exchange in the fitting of PPs. This could also explain the larger PAW-PBE errors for HF relative to those of the tested DFAs. Error distributions for the GTH-PBE approximation in PBE and B97M-rV computations are similar to those for fit-CRENBL: PP errors are significant for both DFAs, but the potential is particularly ill-suited for use with B97M-rV.

Since atomization energies reflect changes in the electronic environment between molecules and atoms, it is possible that a significant part of these large errors can be corrected on an atom-by-atom basis. Indeed, at least one previous report on similar data sets has advocated for atomic correction schemes to ameliorate PP errors in these systems.[127] We define atomic corrections δE_X for atom X, according to

$$E'_X = E_X + \delta E_X \tag{24}$$

where E_X is the uncorrected energy for atom X. Corrections for each DFA/PP pair were optimized by multiple linear regression to minimize the RMSE of the W4-11 and used to recompute TAEs for this set. All values of δE_X are reported in Tables S9−S12. The errors for the corrected PPs are represented by the right-hand distributions of each violin in Figure 4, indicating that significant reductions in PP errors are achieved through atomic corrections. Once corrected, nearly uniform performance across all DFA/PP pairs is achieved, and error distributions are roughly normal. These atomic corrections are specifically fit to the W4-11 set, and we do not necessarily recommend their wide use in other systems without further validation. Nevertheless, the success of this approach indicates that the most egregious errors in atomization energies for unmodified PPs are highly systematic, and simple correction schemes can correct for this in the native and transferred use of PPs.

While element-specific corrections are clearly valuable for atomization energies, these are not directly applicable to more general types of reaction energies. This highlights the need for universal correction schemes for PPs. On the basis of fit-CRENBL results, where high performance in HF and ωB97X-V suggests the importance of exact exchange in PP fitting, we have attempted the use of density-corrected (DC) DFA calculations[128−130] to improve PP errors (Section S2.2 and Figure S3). While these led to minor reductions in the fit-CRENBL error for the remaining four DFAs, this procedure was unable to recover anything near the high performance of the empirical corrections. Others have successfully employed nonlinear core corrections (NLCCs) to reduce PPEs (though not necessarily PP inconsistency errors) in similar systems,[127] and we are currently exploring their use in these systems.

4. SUMMARY AND CONCLUSIONS

The preceding sections have demonstrated that PP errors and PP inconsistency errors are not evenly distributed across all types of molecular energy differences. In particular, we find it helpful to divide these into three categories:

https://doi.org/10.1021/acs.jctc.3c00089
J. Chem. Theory Comput. 2023, 19, 2827−2841

- *The Good.* These are cases where PP errors are minimal relative to that introduced by other approximations in the computation and/or achieve chemical accuracy. They include nonbonded interactions (such as S22 systems[82]) and barrier heights for organometallic reactions (such as TMB11 systems[84,87−91]). There are select cases where PP errors are greater than 1 kcal mol^{-1} for TMB11 predictions, but even the worst of these is about 5 kcal mol^{-1} and errors are much smaller in a statistical sense.
- *The Bad.* Here we include systems where PP errors are significant for enough systems that chemical accuracy is not achieved statistically. We find this to be the case for the transition-metal reaction[84,86] and dimerization[84,85] energies for most of the classes of PPs studied herein. PAW-PBE and def2-ECP RMS PP errors hover right around 1 kcal mol^{-1}, but errors and inconsistency errors for fit-CRENBL and GTH-PBE are 2 to 3 times this large.
- *The Ugly.* For the breaking of main-group bonds (the W4-11 systems[83]), PP inconsistency errors can be strikingly bad. The difference between consistent and inconsistent PP use is most obvious for the fit-CRENBL potential, whereas GTH potentials result in significant errors regardless of the consistency of the protocol. The PAW-PBE potentials as implemented in VASP exhibit the best performance out of the box, and only with use in HF do errors become notable.

Overall, we find that the inconsistent use of PPs represents an often overlooked but potentially serious source of error in modern DFT computations. Based on a relatively small set of results, previous authors have argued that these errors are "much smaller than the errors...introduced by incomplete basis sets"[15] or that "error inherent in the (ab initio) electron correlation or density functional procedure is almost always larger than the error produced by the pseudopotential approximation."[9] However, the results presented here indicate that there are many contexts in which these conclusions are simply not true. Particular care should be taken when PPs are used in circumstances that break main-group bonds, and potentials such as def2-ECP, where elements in the first three rows of the periodic table are all-electron, are strongly recommended where possible.

This work has additional implications for the development of PPs and even density functionals. First, results for the W4-11 set indicate that PP inconsistency errors for atomization energies are extremely systematic, and a single energy correction for each atom can remove them almost entirely. Others have come to similar conclusions.[127] There may also be scope for the development of generalizations of this approach that permit application to classes of chemical energy differences beyond atomization energies.

However, it is more desirable to instead pursue corrections to the PP formalism itself. Nonlinear core corrections (NLCCs) represent one possible path forward,[10,127] and we are exploring their use in mitigating inconsistency errors.

Additionally, the results of this study indicate that PP inconsistency errors do not plague all DFAs equally. Specifically, B97M-rV meta-GGA seems to be particularly susceptible to PP errors. We have not explored the reason for this, but it is possible that the excellent performance of this functional for main-group thermochemistry[100,101] is accompanied by greater sensitivity to the representation of the density. More broadly, differential inconsistency errors between DFAs suggest the possibility that performance in PP calculations should be considered in the course of future DFA design; this would be relatively straightforward by including energy differences evaluated with and without the use of PPs in training, validation, and test sets.

■ ASSOCIATED CONTENT

Supporting Information

The Supporting Information is available free of charge at https://pubs.acs.org/doi/10.1021/acs.jctc.3c00089.

Raw data for benchmark computations with various DFAs and PPs (XLSX)

Additional benchmarking calculations, statistics, and parameters for PP atom corrections (PDF)

Machine-readable version of SI tables (XLSX)

■ AUTHOR INFORMATION

Corresponding Author

Martin Head-Gordon − *Kenneth S. Pitzer Center for Theoretical Chemistry, Department of Chemistry, University of California, Berkeley, California 94720, United States; Department of Chemistry, University of California, Berkeley, California 94720, United States; Chemical Sciences Division, Lawrence Berkeley National Laboratory, Berkeley, California 94720, United States;* orcid.org/0000-0002-4309-6669; Phone: +1 (510)642-5957; Email: mhg@cchem.berkeley.edu; Fax: +1 (510)643-1255

Authors

Elliot Rossomme − *Kenneth S. Pitzer Center for Theoretical Chemistry, Department of Chemistry, University of California, Berkeley, California 94720, United States; Department of Chemistry, University of California, Berkeley, California 94720, United States; Chemical Sciences Division, Lawrence Berkeley National Laboratory, Berkeley, California 94720, United States;* orcid.org/0000-0002-4727-0652

Leonardo A. Cunha − *Kenneth S. Pitzer Center for Theoretical Chemistry, Department of Chemistry, University of California, Berkeley, California 94720, United States; Chemical Sciences Division, Lawrence Berkeley National Laboratory, Berkeley, California 94720, United States;* orcid.org/0000-0003-2671-2375

Wanlu Li − *Kenneth S. Pitzer Center for Theoretical Chemistry, Department of Chemistry, University of California, Berkeley, California 94720, United States; Department of Chemistry, University of California, Berkeley, California 94720, United States; Chemical Sciences Division, Lawrence Berkeley National Laboratory, Berkeley, California 94720, United States;* orcid.org/0000-0003-0098-0670

Kaixuan Chen − *Kenneth S. Pitzer Center for Theoretical Chemistry, Department of Chemistry, University of California, Berkeley, California 94720, United States; Department of Chemistry, University of California, Berkeley, California 94720, United States; Chemical Sciences Division, Lawrence Berkeley National Laboratory, Berkeley, California 94720, United States;* orcid.org/0000-0002-7864-7440

Alexandra R. McIsaac − *Kenneth S. Pitzer Center for Theoretical Chemistry, Department of Chemistry, University of California, Berkeley, California 94720, United States; Department of Chemistry, University of California, Berkeley,*

California 94720, United States; Chemical Sciences Division, Lawrence Berkeley National Laboratory, Berkeley, California 94720, United States; orcid.org/0000-0002-7210-1164

Teresa Head-Gordon − *Kenneth S. Pitzer Center for Theoretical Chemistry, Department of Chemistry, University of California, Berkeley, California 94720, United States; Department of Chemistry, Department of Bioengineering, and Department of Chemical and Biomolecular Engineering, University of California, Berkeley, California 94720, United States; Chemical Sciences Division, Lawrence Berkeley National Laboratory, Berkeley, California 94720, United States;* orcid.org/0000-0003-0025-8987

Complete contact information is available at: https://pubs.acs.org/10.1021/acs.jctc.3c00089

Notes

The authors declare the following competing financial interest(s): M.H.-G. is a part owner of Q-Chem Inc., whose software was used for many of the calculations reported here.

■ ACKNOWLEDGMENTS

This work was supported by the U.S. Department of Energy, Office of Science, Office of Advanced Scientific Computing, and Office of Basic Energy Sciences via the Scientific Discovery through Advanced Computing (SciDAC) program.

■ REFERENCES

(1) Hellmann, H. A new approximation method in the problem of many electrons. *J. Chem. Phys.* **1935**, *3*, 61−61.
(2) Phillips, J. C. Energy-Band Interpolation Scheme Based on a Pseudopotential. *Phys. Rev.* **1958**, *112*, 685−695.
(3) Phillips, J. C.; Kleinman, L. New Method for Calculating Wave Functions in Crystals and Molecules. *Phys. Rev.* **1959**, *116*, 287−294.
(4) Pickett, W. E. Pseudopotential methods in condensed matter applications. *Comput. Phys. Rep.* **1989**, *9*, 115−197.
(5) Weeks, J. D.; Rice, S. A. Use of Pseudopotentials in Atomic-Structure Calculations. *J. Chem. Phys.* **1968**, *49*, 2741−2755.
(6) Dolg, M.; Cao, X. Relativistic pseudopotentials: their development and scope of applications. *Chem. Rev.* **2012**, *112*, 403−480.
(7) Tuckerman, M. E. Ab initio molecular dynamics: basic concepts, current trends and novel applications. *J. Phys.: Condens. Matter* **2002**, *14*, R1297.
(8) Kirchner, B.; di Dio, P. J.; Hutter, J. In *Multiscale Molecular Methods in Applied Chemistry*; Kirchner, B., Vrabec, J., Eds.; Springer: Berlin, 2012; pp 109−153.
(9) Schwerdtfeger, P. The pseudopotential approximation in electronic structure theory. *ChemPhysChem* **2011**, *12*, 3143−3155.
(10) Goedecker, S.; Saha, S. In *Handbook of Solid State Chemistry*; Dronskowski, R., Kikkawa, S., Stein, A., Eds.; Wiley-VCH Verlag GmbH & Co, 2017; Chapter 2, pp 29−58.
(11) Christiansen, P. A.; Lee, Y. S.; Pitzer, K. S. Improved ab initio effective core potentials for molecular calculations. *J. Chem. Phys.* **1979**, *71*, 4445.
(12) Andrae, D.; Haußermann, U.; Dolg, M.; Stoll, H.; Preuss, H. Energy-adjusted ab initio pseudopotentials for the second and third row transition elements. *Theor. Chim. Acta* **1990**, *77*, 123−141.
(13) Blöchl, P. E. Projector augmented-wave method. *Phys. Rev. B* **1994**, *50*, 17953−17979.
(14) Goedecker, S.; Teter, M.; Hutter, J. Separable dual-space Gaussian pseudopotentials. *Phys. Rev. B* **1996**, *54*, 1703−1710.
(15) Hartwigsen, C.; Goedecker, S.; Hutter, J. Relativistic separable dual-space Gaussian pseudopotentials from H to Rn. *Phys. Rev. B* **1998**, *58*, 3641−3662.
(16) Bachelet, G. B.; Hamann, D. R.; Schlüter, M. Pseudopotentials that work: From H to Pu. *Phys. Rev. B* **1982**, *26*, 4199−4228.
(17) Krack, M. Pseudopotentials for H to Kr optimized for gradient-corrected exchange-correlation functions. *Theor. Chem. Acc.* **2005**, *114*, 145−152.
(18) Tan, H.; Li, Y.; Zhang, S. B.; Duan, W. Effect of Hartree−Fock pseudopotentials on local density functional theory calculations. *Phys. Chem. Chem. Phys.* **2018**, *20*, 18844−18849.
(19) Yang, J.; Tan, L. Z.; Rappe, A. M. Hybrid functional pseudopotentials. *Phys. Rev. B* **2018**, *97*, 085130.
(20) Li, W.-L.; Chen, K.; Rossomme, E.; Head-Gordon, M.; Head-Gordon, T. Optimized pseudopotentials and basis sets for semi-empirical density functional theory for electrocatalysis applications. *J. Phys. Chem. Lett.* **2021**, *12*, 10304−10309.
(21) van Wüllen, C. On the use of common effective core potentials in density functional calculations. I. Test calculations on transition-metal carbonyls. *Int. J. Quantum Chem.* **1996**, *58*, 147−152.
(22) Hay, P. J.; Martin, R. L. Theoretical studies of the structures and vibrational frequencies of actinide compounds using relativistic effective core potentials with Hartree−Fock and density functional methods: UF 6, NpF 6, and PuF 6. *J. Chem. Phys.* **1998**, *109*, 3875−3881.
(23) Russo, T. V.; Martin, R. L.; Hay, P. J. Effective core potentials for DFT calculations. *J. Phys. Chem.* **1995**, *99*, 17085−17087.
(24) Hay, P. J.; Wadt, W. R. Ab initio effective core potentials for molecular calculations. Potentials for K to Au including the outermost core orbitals. *J. Chem. Phys.* **1985**, *82*, 299−310.
(25) Fuchs, M.; Bockstedte, M.; Pehlke, E.; Scheffler, M. Pseudopotential study of binding properties of solids within generalized gradient approximations: The role of core-valence exchange correlation. *Phys. Rev. B* **1998**, *57*, 2134−2145.
(26) De Jong, W. A.; Harrison, R. J.; Nichols, J. A.; Dixon, D. A. Fully relativistic correlated benchmark results for uranyl and a critical look at relativistic effective core potentials for uranium. *Theor. Chem. Acc.* **2001**, *107*, 22−26.
(27) Roy, L. E.; Hay, P. J.; Martin, R. L. Revised basis sets for the LANL effective core potentials. *J. Chem. Theory Comput.* **2008**, *4*, 1029−1031.
(28) Aebersold, L. E.; Yuwono, S. H.; Schoendorff, G.; Wilson, A. K. Efficacy of density functionals and relativistic effective core potentials for lanthanide-containing species: The Ln54 molecule set. *J. Chem. Theory Comput.* **2017**, *13*, 2831−2839.
(29) Borlido, P.; Doumont, J.; Tran, F.; Marques, M. A. L.; Botti, S. Validation of pseudopotential calculations for the electronic band gap of solids. *J. Chem. Theory Comput.* **2020**, *16*, 3620−3627.
(30) Rauch, T.; Marques, M. A. L.; Botti, S. Electronic structure of molecules, surfaces, and molecules on surfaces with the local modified Becke−Johnson exchange−correlation potential. *J. Chem. Theory Comput.* **2021**, *17*, 4746−4755.
(31) Wu, Y.; Jiang, Z.; Tan, H.; Li, Y.; Duan, W. Accuracy trade-off between one-electron and excitonic spectra of cuprous halides in first-principles calculations. *J. Chem. Phys.* **2021**, *154*, 134704.
(32) van Setten, M.; Giantomassi, M.; Bousquet, E.; Verstraete, M.; Hamann, D.; Gonze, X.; Rignanese, G.-M. The PseudoDojo: Training and grading a 85 element optimized norm-conserving pseudopotential table. *Comput. Phys. Commun.* **2018**, *226*, 39−54.
(33) Cunha, L. A.; Hait, D.; Kang, R.; Mao, Y.; Head-Gordon, M. Relativistic orbital-optimized density functional theory for accurate core-level spectroscopy. *J. Phys. Chem. Lett.* **2022**, *13*, 3438−3449.
(34) Cao, X.; Dolg, M. Pseudopotentials and modelpotentials. *Wiley Interdiscip. Rev.: Comput. Mol. Sci.* **2011**, *1*, 200−210.
(35) Kahn, L. R.; Goddard, W. A., III Ab initio effective potentials for use in molecular calculations. *J. Chem. Phys.* **1972**, *56*, 2685−2701.
(36) Kleinman, L. Relativistic norm-conserving pseudopotential. *Phys. Rev. B* **1980**, *21*, 2630−2631.
(37) Kutzelnigg, W. The relativistic many body problem in molecular theory. *Phys. Scr.* **1987**, *36*, 416.
(38) Ermler, W. C.; Lee, Y. S.; Pitzer, K. S.; Winter, N. W. A binitio effective core potentials including relativistic effects. II. Potential energy curves for Xe2, Xe+ 2, and Xe* 2. *J. Chem. Phys.* **1978**, *69*, 976−983.

(39) Hafner, P.; Schwarz, W. Molecular spinors from the quasi-relativistic pseudopotential approach. *Chem. Phys. Lett.* **1979**, *65*, 537−541.
(40) Ermler, W. C.; Lee, Y. S.; Christiansen, P. A.; Pitzer, K. S. AB initio effective core potentials including relativistic effects. A procedure for the inclusion of spin-orbit coupling in molecular wavefunctions. *Chem. Phys. Lett.* **1981**, *81*, 70−74.
(41) Pitzer, R. M.; Winter, N. W. Electronic-structure methods for heavy-atom molecules. *J. Phys. Chem.* **1988**, *92*, 3061−3063.
(42) Schwarz, W. The general form of pseudopotential operators. *Theor. Chim. Acta* **1971**, *23*, 147−154.
(43) Chang, T.; Habitz, P.; Pittel, B.; Schwarz, W. Accuracy and limitations of the pseudopotential method. *Theor. Chim. Acta* **1974**, *34*, 263−275.
(44) Hamann, D. R.; Schlüter, M.; Chiang, C. Norm-Conserving Pseudopotentials. *Phys. Rev. Lett.* **1979**, *43*, 1494−1497.
(45) Kleinman, L. Relativistic norm-conserving pseudopotential. *Phys. Rev. B* **1980**, *21*, 2630−2631.
(46) Shirley, E. L.; Allan, D. C.; Martin, R. M.; Joannopoulos, J. D. Extended norm-conserving pseudopotentials. *Phys. Rev. B* **1989**, *40*, 3652−3660.
(47) Teter, M. Additional condition for transferability in pseudopotentials. *Phys. Rev. B* **1993**, *48*, 5031−5041.
(48) Goedecker, S.; Maschke, K. Transferability of pseudopotentials. *Phys. Rev. A* **1992**, *45*, 88−93.
(49) Trail, J. R.; Needs, R. J. Norm-conserving Hartree−Fock pseudopotentials and their asymptotic behavior. *J. Chem. Phys.* **2005**, *122*, 014112.
(50) Trail, J.; Needs, R. Smooth relativistic Hartree−Fock pseudopotentials for H to Ba and Lu to Hg. *J. Chem. Phys.* **2005**, *122*, 174109.
(51) Kahn, L. R.; Baybutt, P.; Truhlar, D. G. Ab initio effective core potentials: Reduction of all-electron molecular structure calculations to calculations involving only valence electrons. *J. Chem. Phys.* **1976**, *65*, 3826−3853.
(52) Stevens, W. J.; Krauss, M.; Basch, H.; Jasien, P. G. Relativistic compact effective potentials and efficient, shared-exponent basis sets for the third-, fourth-, and fifth-row atoms. *Can. J. Chem.* **1992**, *70*, 612−630.
(53) Dolg, M.; Wedig, U.; Stoll, H.; Preuss, H. Energy-adjusted abinitio pseudopotentials for the first row transition elements. *J. Chem. Phys.* **1987**, *86*, 866−872.
(54) Küchle, W.; Dolg, M.; Stoll, H.; Preuss, H. Ab initio pseudopotentials for Hg through Rn. *Mol. Phys.* **1991**, *74*, 1245−1263.
(55) Topp, W. C.; Hopfield, J. J. Chemically motivated pseudopotential for sodium. *Phys. Rev. B* **1973**, *7*, 1295.
(56) Hay, P. J.; Wadt, W. R.; Kahn, L. R. Ab initio effective core potentials for molecular calculations. II. All-electron comparisons and modifications of the procedure. *J. Chem. Phys.* **1978**, *68*, 3059−3066.
(57) Fernandez Pacios, L.; Christiansen, P. A. Ab initio relativistic effective potentials with spin-orbit operators. I. Li through Ar. *J. Chem. Phys.* **1985**, *82*, 2664−2671.
(58) Hurley, M. M.; PAcios, L. F.; Christiansen, P. A.; Ross, R. B.; Ermler, W. C. Ab initio relativistic effective potentials with spin-orbit operators. II. K through Kr. *J. Chem. Phys.* **1986**, *84*, 6840−6853.
(59) LaJohn, L. A.; Christiansen, P. A.; Ross, R. B.; Atashroo, T.; Ermler, W. C. Ab initio relativistic effective potentials with spin−orbit operators. III. Rb through Xe. *J. Chem. Phys.* **1987**, *87*, 2812−2824.
(60) Ross, R. B.; Powers, J. M.; Atashroo, T.; Ermler, W. C.; LaJohn, L. A.; Christiansen, P. A. Ab initio relativistic effective potentials with spin−orbit operators. IV. Cs through Rn. *J. Chem. Phys.* **1990**, *93*, 6654−6670.
(61) McKenzie, S. C.; Epifanovsky, E.; Barca, G. M. J.; Gilbert, A. T. B.; Gill, P. M. W. Efficient method for calculating effective core potential integrals. *J. Phys. Chem. A* **2018**, *122*, 3066−3075.
(62) Bergner, A.; Dolg, M.; Küchle, W.; Stoll, H.; Preuß, H. Ab initio energy-adjusted pseudopotentials for elements of groups 13−17. *Mol. Phys.* **1993**, *80*, 1431−1441.
(63) Fuentealba, P.; Stoll, H.; von Szentpaly, L.; Schwerdtfeger, P.; Preuss, H. On the reliability of semi-empirical pseudopotentials: simulation of Hartree−Fock and Dirac-Fock results. *J. Phys. B: At. Mol. Phys.* **1983**, *16*, L323.
(64) Fuentealba, P.; von Szentpaly, L.; Preuss, H.; Stoll, H. Pseudopotential calculations for alkaline-earth atoms. *J. Phys. B: At. Mol. Phys.* **1985**, *18*, 1287.
(65) Igel-Mann, G.; Stoll, H.; Preuss, H. Pseudopotentials for main group elements (IIIa through VIIa). *Mol. Phys.* **1988**, *65*, 1321−1328.
(66) Dolg, M.; Stoll, H.; Preuss, H. Energy-adjusted ab initio pseudopotentials for the rare earth elements. *J. Chem. Phys.* **1989**, *90*, 1730−1734.
(67) Andrae, D.; Häußermann, U.; Dolg, M.; Stoll, H.; Preuß, H. Energy-adjusted ab initio pseudopotentials for the second and third row transition elements: Molecular test for M_2 (M = Ag, Au) and MH (M = Ru, Os). *Theor. Chim. Acta* **1991**, *78*, 247−266.
(68) Weigend, F.; Furche, F.; Ahlrichs, R. Gaussian basis sets of quadruple zeta valence quality for atoms H-Kr. *J. Chem. Phys.* **2003**, *119*, 12753.
(69) Weigend, F.; Ahlrichs, R. Balanced basis sets of split valence, triple zeta valence, and quadruple valence quality for H to Rn: Design and assessment of accuracy. *Phys. Chem. Chem. Phys.* **2005**, *7*, 3297−3305.
(70) Kaupp, M.; Schleyer, P. v. R.; Stoll, H.; Preuss, H. Pseudopotential approaches to Ca, Sr, and Ba hydrides. Why are some alkaline earth MX2 compounds bent? *J. Chem. Phys.* **1991**, *94*, 1360−1366.
(71) Leininger, T.; Nicklass, A.; Küchle, W.; Stoll, H.; Dolg, M.; Bergner, A. The accuracy of the pseudopotential approximation: Non-frozen-core effects for spectroscopic constants of alkali fluorides XF (X= K, Rb, Cs). *Chem. Phys. Lett.* **1996**, *255*, 274−280.
(72) Metz, B.; Stoll, H.; Dolg, M. Small-core multiconfiguration-Dirac−Hartree−Fock-adjusted pseudopotentials for post-d main group elements: Application to PbH and PbO. *J. Chem. Phys.* **2000**, *113*, 2563−2569.
(73) Peterson, K. A.; Figgen, D.; Goll, E.; Stoll, H.; Dolg, M. Systematically convergent basis sets with relativistic pseudopotentials. II. Small-core pseudopotentials and correlation consistent basis sets for the post-d group 16−18 elements. *J. Chem. Phys.* **2003**, *119*, 11113−11123.
(74) Lu, J.-B.; Cantu, D. C.; Nguyen, M.-T.; Li, J.; Glezakou, V.-A.; Rousseau, R. Norm-conserving pseudopotentials and basis sets to explore lanthanide chemistry in complex environments. *J. Chem. Theory Comput.* **2019**, *15*, 5987−5997.
(75) Lu, J.-B.; Cantu, D. C.; Xu, C.-Q.; Nguyen, M.-T.; Hu, H.-S.; Glezakou, V.-A.; Rousseau, R.; Li, J. Norm-conserving pseudopotentials and basis sets to explore actinide chemistry in complex environments. *J. Chem. Theory Comput.* **2021**, *17*, 3360−3371.
(76) Kresse, G.; Joubert, D. From ultrasoft pseudopotentials to the projector augmented-wave method. *Phys. Rev. B* **1999**, *59*, 1758−1775.
(77) Hafner, J. Ab-initio simulations of materials using VASP: Density-functional theory and beyond. *J. Comput. Chem.* **2008**, *29*, 2044−2078.
(78) Sun, J.; Marsman, M.; Csonka, G. I.; Ruzsinszky, A.; Hao, P.; Kim, Y.-S.; Kresse, G.; Perdew, J. P. Self-consistent meta-generalized gradient approximation within the projector-augmented-wave method. *Phys. Rev. B* **2011**, *84*, 035117.
(79) Kühne, T. D.; Iannuzzi, M.; Del Ben, M.; Rybkin, V. V.; Seewald, P.; Stein, F.; Laino, T.; Khaliullin, R. Z.; Schütt, O.; Schiffmann, F.; Golze, D.; Wilhelm, J.; Chulkov, S.; Bani-Hashemian, M. H.; Weber, V.; Borštnik, U.; Taillefumier, M.; Jakobovits, A. S.; Lazzaro, A.; Pabst, H.; Müller, T.; Schade, R.; Guidon, M.; Andermatt, S.; Holmberg, N.; Schenter, G. K.; Hehn, A.; Bussy, A.; Belleflamme, F.; Tabacchi, G.; Glöß, A.; Lass, M.; Bethune, I.; Mundy, C. J.; Plessl, C.; Watkins, M.; VandeVondele, J.; Krack, M.; Hutter, J. CP2K: An electronic structure and molecular dynamics software package - Quickstep: Efficient and accurate electronic structure calculations. *J. Chem. Phys.* **2020**, *152*, 194103.

https://doi.org/10.1021/acs.jctc.3c00089
J. Chem. Theory Comput. 2023, 19, 2827−2841

(80) Lininger, C. N.; Gauthier, J. A.; Li, W.-L.; Rossomme, E.; Welborn, V. V.; Lin, Z.; Head-Gordon, T.; Head-Gordon, M.; Bell, A. T. Challenges for density functional theory: calculation of CO adsorption on electrocatalytically relevant metals. *Phys. Chem. Chem. Phys.* **2021**, *23*, 9394−9406.
(81) Andrae, D.; Häußermann, U.; Dolg, M.; Stoll, H.; Preuß, H. Energy-adjusted *ab initio* pseudopotentials for the second and third row transition elements. *Theor. Chim. Acta* **1990**, *77*, 123−141.
(82) Jurečka, P.; Šponer, J.; Černý, J.; Hobza, P. Benchmark database of accurate MP2 and CCSD(T) complete basis set limit interaction energies of small model complexes, DNA base pairs, and amino acid pairs. *Phys. Chem. Chem. Phys.* **2006**, *8*, 1985−1993.
(83) Karton, A.; Daon, S.; Martin, J. M. L. W4−11: A high-confidence benchmark dataset for computational thermochemistry dervied from first-principles W4 data. *Chem. Phys. Lett.* **2011**, *510*, 165−178.
(84) Chan, B.; Gill, P. M. W.; Kimura, M. Assessment of DFT methods for transition metals with the TMC151 compilation of data sets and comparison with accuracies for main-group chemistry. *J. Chem. Theory Comput.* **2019**, *15*, 3610−3622.
(85) Moltved, K. A.; Kepp, K. P. Chemical bond energies of 3d transition metals studied by density functional theory. *J. Chem. Theory Comput.* **2018**, *14*, 3479−3492.
(86) Chan, B. Formulation of small test sets using large test sets for efficient assessment of quantum chemistry methods. *J. Chem. Theory Comput.* **2018**, *14*, 4254−4262.
(87) Kang, R.; Lai, W.; Yao, J.; Shaik, S.; Chen, H. How accurate can a local couped cluster approach be in computing the activation energies of late-transition-metal-catalyzed reactions with Au, Pt, and Ir? *J. Chem. Theory Comput.* **2012**, *8*, 3119−3127.
(88) Sun, Y.; Chen, H. Performance of density functionals for activation energies of Zr-mediated reactions. *J. Chem. Theory Comput.* **2013**, *9*, 4735−4743.
(89) Sun, Y.; Chen, H. Performance of density functionals for activation energies of Re-catalyzed organic reactions. *J. Chem. Theory Comput.* **2014**, *10*, 579−588.
(90) Hu, L.; Chen, H. Assessment of DFT methods for computing activation energies of Mo/W-mediated reactions. *J. Chem. Theory Comput.* **2015**, *11*, 4601−4614.
(91) Dohm, S.; Hansen, A.; Steinmetz, M.; Grimme, S.; Checinski, M. P. Comprehensive thermochemical benchmark set of realistic closed-shell metal organic reactions. *J. Chem. Theory Comput.* **2018**, *14*, 2596−2608.
(92) Fuentealba, P.; von Szentpály, L.; Preuss, H.; Stoll, H. Pseudopotential calculations for alkaline-earth atoms. *J. Phys. B: At. Mol. Phys.* **1985**, *18*, 1287−1296.
(93) Roothaan, C. C. J. New developments in molecular orbital theory. *Rev. Mod. Phys.* **1951**, *23*, 69−89.
(94) Hall, G. G. The molecular orbital theory of chemical valency VIII. A method of calculating ionization potentials. *Proc. R. Soc. Lond. A* **1951**, *205*, 541−552.
(95) Pople, J. A.; Nesbet, R. K. Self-consistent orbitals for radicals. *J. Chem. Phys.* **1954**, *22*, 571−572.
(96) Berthier, G. Extension de la méthode du champ moléculaire self-consistent à l'étude des états à couches incompletes. *C. R. Hebd. Seances Acad. Sci.* **1954**, *238*, 91−93.
(97) Vosko, S. H.; Wilk, L.; Nusair, M. Accurate spin-dependent electron liquid correlation energies for local spin density calculations: A critical analysis. *Can. J. Phys.* **1980**, *58*, 1200−1211.
(98) Perdew, J. P.; Burke, K.; Ernzerhof, M. Generalized gradient approximation made simple. *Phys. Rev. Lett.* **1996**, *77*, 3865−3868.
(99) Sun, J.; Ruzsinszky, A.; Perdew, J. P. Strongly constrained and appropriately normed semilocal density functional. *Phys. Rev. Lett.* **2015**, *115*, 036402.
(100) Mardirossian, N.; Head-Gordon, M. Mapping the genome of meta-generalized gradient approximation density functionals: The search for B97M-V. *J. Chem. Phys.* **2015**, *142*, 074111.
(101) Mardirossian, N.; Pestana, L. R.; Womack, J. C.; Skylaris, C.-K.; Head-Gordon, T.; Head-Gordon, M. Use of the rVV10 nonlocal correlation functional in the B97M-V density functional: Defining B97M-rV and related functionals. *J. Phys. Chem. Lett.* **2017**, *8*, 35−40.
(102) Mardirossian, N.; Head-Gordon, M. *Phys. Chem. Chem. Phys.* **2014**, *16*, 9904−9924.
(103) Epifanovsky, E.; Gilbert, A. T. B.; Feng, X.; Lee, J.; Mao, Y.; Mardirossian, N.; Pokhilko, P.; White, A. F.; Coons, M. P.; Dempwolff, A. L.; Gan, Z.; Hait, D.; Horn, P. R.; Jacobson, L. D.; Kaliman, I.; Kussmann, J.; Lange, A. W.; Lao, K. U.; Levine, D. S.; Liu, J.; McKenzie, S. C.; Morrison, A. F.; Nanda, K. D.; Plasser, F.; Rehn, D. R.; Vidal, M. L.; You, Z.-Q.; Zhu, Y.; Alam, B.; Albrecht, B. J.; Aldossary, A.; Alguire, E.; Andersen, J. H.; Athavale, V.; Barton, D.; Begam, K.; Behn, A.; Bellonzi, N.; Bernard, Y. A.; Berquist, E. J.; Burton, H. G. A.; Carreras, A.; Carter-Fenk, K.; Chakraborty, R.; Chien, A. D.; Closser, K. D.; Cofer-Shabica, V.; Dasgupta, S.; de Wergifosse, M.; Deng, J.; Diedenhofen, M.; Do, H.; Ehlert, S.; Fang, P.-T.; Fatehi, S.; Feng, Q.; Friedhoff, T.; Gayvert, J.; Ge, Q.; Gidofalvi, G.; Goldey, M.; Gomes, J.; González-Espinoza, C. E.; Gulania, S.; Gunina, A. O.; Hanson-Heine, M. W. D.; Harbach, P. H. P.; Hauser, A.; Herbst, M. F.; Hernández Vera, M.; Hodecker, M.; Holden, Z. C.; Houck, S.; Huang, X.; Hui, K.; Huynh, B. C.; Ivanov, M.; Jász, A.; Ji, H.; Jiang, H.; Kaduk, B.; Kähler, S.; Khistyaev, K.; Kim, J.; Kis, G.; Klunzinger, P.; Koczor-Benda, Z.; Koh, J. H.; Kosenkov, D.; Koulias, L.; Kowalczyk, T.; Krauter, C. M.; Kue, K.; Kunitsa, A.; Kus, T.; Ladjánszki, I.; Landau, A.; Lawler, K. V.; Lefrancois, D.; Lehtola, S.; Li, R. R.; Li, Y.-P.; Liang, J.; Liebenthal, M.; Lin, H.-H.; Lin, Y.-S.; Liu, F.; Liu, K.-Y.; Loipersberger, M.; Luenser, A.; Manjanath, A.; Manohar, P.; Mansoor, E.; Manzer, S. F.; Mao, S.-P.; Marenich, A. V.; Markovich, T.; Mason, S.; Maurer, S. A.; McLaughlin, P. F.; Menger, M. F. S. J.; Mewes, J.-M.; Mewes, S. A.; Morgante, P.; Mullinax, J. W.; Oosterbaan, K. J.; Paran, G.; Paul, A. C.; Paul, S. K.; Pavošević, F.; Pei, Z.; Prager, S.; Proynov, E. I.; Rák, A.; Ramos-Cordoba, E.; Rana, B.; Rask, A. E.; Rettig, A.; Richard, R. M.; Rob, F.; Rossomme, E.; Scheele, T.; Scheurer, M.; Schneider, M.; Sergueev, N.; Sharada, S. M.; Skomorowski, W.; Small, D. W.; Stein, C. J.; Su, Y.-C.; Sundstrom, E. J.; Tao, Z.; Thirman, J.; Tornai, G. J.; Tsuchimochi, T.; Tubman, N. M.; Veccham, S. P.; Vydrov, O.; Wenzel, J.; Witte, J.; Yamada, A.; Yao, K.; Yeganeh, S.; Yost, S. R.; Zech, A.; Zhang, I. Y.; Zhang, X.; Zhang, Y.; Zuev, D.; Aspuru-Guzik, A.; Bell, A. T.; Besley, N. A.; Bravaya, K. B.; Brooks, B. R.; Casanova, D.; Chai, J.-D.; Coriani, S.; Cramer, C. J.; Cserey, G.; DePrince, A. E.; DiStasio, R. A.; Dreuw, A.; Dunietz, B. D.; Furlani, T. R.; Goddard, W. A.; Hammes-Schiffer, S.; Head-Gordon, T.; Hehre, W. J.; Hsu, C.-P.; Jagau, T.-C.; Jung, Y.; Klamt, A.; Kong, J.; Lambrecht, D. S.; Liang, W.; Mayhall, N. J.; McCurdy, C. W.; Neaton, J. B.; Ochsenfeld, C.; Parkhill, J. A.; Peverati, R.; Rassolov, V. A.; Shao, Y.; Slipchenko, L. V.; Stauch, T.; Steele, R. P.; Subotnik, J. E.; Thom, A. J. W.; Tkatchenko, A.; Truhlar, D. G.; Van Voorhis, T.; Wesolowski, T. A.; Whaley, K. B.; Woodcock, H. L.; Zimmerman, P. M.; Faraji, S.; Gill, P. M. W.; Head-Gordon, M.; Herbert, J. M.; Krylov, A. I. Software for the frontiers of quantum chemistry: An overview of developments in the Q-Chem 5 package. *J. Chem. Phys.* **2021**, *155*, 084801.
(104) Rappoport, D.; Furche, F. Property-optimized Gaussian basis sets for molecular response calculations. *J. Chem. Phys.* **2010**, *133*, 134105.
(105) Krishnan, R.; Binkley, J. S.; Seeger, R.; Pople, J. A. Self-consistent molecular orbital methods. XX. A basis set for correlated wave functions. *J. Chem. Phys.* **1980**, *72*, 650−654.
(106) Frisch, M. J.; Pople, J. A.; Binkley, J. S. Self-consistent molecular orbital methods 25. Supplementary functions for Gaussian basis sets. *J. Chem. Phys.* **1984**, *80*, 3265−3269.
(107) Lebedev, V. I. Values of the nodes and weights of ningth to seventeenth order gauss-markov quadrature formulae invariant under the octahedron group with inversion. *USSR Comput. Math. Math. Phys.* **1975**, *15*, 44−51.
(108) Lebedev, V. I. Quadratures on a sphere. *USSR Comput. Math. Math. Phys.* **1976**, *16*, 10−24.
(109) VandeVondele, J.; Krack, M.; Mohamed, F.; Parrinello, M.; Chassaing, T.; Hutter, J. Quickstep: Fast and accurate density

https://doi.org/10.1021/acs.jctc.3c00089
J. Chem. Theory Comput. 2023, 19, 2827−2841

functional calculations using a mixed Gaussian and plane waves approach. *Comput. Phys. Commun.* **2005**, *167*, 103−128.
(110) Lippert, G.; Hutter, J.; Parrinello, M. A hybrid Gaussian and plane wave density functional scheme. *Mol. Phys.* **1997**, *92*, 477−488.
(111) Hutter, J.; Iannuzzi, M.; Schiffmann, F.; VandeVondele, J. CP2K: Atomistic simulations of condensed matter systems. *Wiley Interdiscip. Rev. Comput. Mol. Sci.* **2014**, *4*, 15−25.
(112) VandeVondele, J.; Hutter, J. Gaussian basis sets for accurate calculations on molecular systems in gas and condensed phases. *J. Chem. Phys.* **2007**, *127*, 114105.
(113) VandeVondele, J.; Hutter, J. An efficient orbital transformation method for electronic structure calculations. *J. Chem. Phys.* **2003**, *118*, 4365−4369.
(114) Kresse, G.; Hafner, J. Ab initio molecular dynamics for open-shell transition metals. *Phys. Rev. B* **1993**, *48*, 13115−13118.
(115) Papajak, E.; Leverentz, H. R.; Zheng, J.; Truhlar, D. G. Efficient Diffuse Basis Sets: cc-pV x Z+ and maug-cc-pV x Z. *J. Chem. Theory Comput.* **2009**, *5*, 1197−1202.
(116) Papajak, E.; Zheng, J.; Xu, X.; Leverentz, H. R.; Truhlar, D. G. Perspectives on basis sets beautiful: Seasonal plantings of diffuse basis functions. *J. Chem. Theory Comput.* **2011**, *7*, 3027−3034.
(117) Liu, W.; Peng, D. Exact two-component Hamiltonians revisited. *J. Chem. Phys.* **2009**, *131*, 031104.
(118) Dyall, K. G. Interfacing relativistic and nonrelativistic methods. I. Normalized elimination of the small component in the modified Dirac equation. *J. Chem. Phys.* **1997**, *106*, 9618−9626.
(119) Saue, T. Relativistic Hamiltonians for chemistry: A primer. *ChemPhysChem* **2011**, *12*, 3077−3094.
(120) Li, Z.; Xiao, Y.; Liu, W. On the spin separation of algebraic two-component relativistic Hamiltonians. *J. Chem. Phys.* **2012**, *137*, 154114.
(121) Cheng, L.; Gauss, J.; Ruscic, B.; Armentrout, P. B.; Stanton, J. F. Bond dissociation energies for diatomic molecules containing 3d transition metals: benchmark scalar-relativistic coupled-cluster calculations for 20 molecules. *J. Chem. Theory Comput.* **2017**, *13*, 1044−1056.
(122) Pollak, P.; Weigend, F. Segmented contracted error-consistent basis sets of double-and triple-ζ valence quality for one-and two-component relativistic all-electron calculations. *J. Chem. Theory Comput.* **2017**, *13*, 3696−3705.
(123) Mardirossian, N.; Head-Gordon, M. Thirty years of density functional theory in computational chemistry: an overview and extensive assessment of 200 density functionals. *Mol. Phys.* **2017**, *115*, 2315−2372.
(124) Neugebauer, J.; Scheffler, M. Adsorbate-substrate and adsorbate-adsorbate interactions of Na and K adlayers on Al(111). *Phys. Rev. B* **1992**, *46*, 16067−16080.
(125) Makov, G.; Payne, M. C. Periodic boundary conditions in ab initio calculations. *Phys. Rev. B* **1995**, *51*, 4014−4022.
(126) Lejaeghere, K.; Bihlmayer, G.; Björkman, T.; Blaha, P.; Blügel, S.; Blum, V.; Caliste, D.; Castelli, I. E.; Clark, S. J.; Dal Corso, A.; de Gironcoli, S.; Deutsch, T.; Kay Dewhurst, J.; Di Marco, I.; Draxl, C.; Dułak, M.; Eriksson, O.; Flores-Livas, J. A.; Garrity, K. F.; Genovese, L.; Giannozzi, P.; Giantomassi, M.; Goedecker, S.; Gonze, X.; Grånäs, O.; U Gross, E. K.; Gulans, A.; Gygi, F.; Hamann, D. R.; Hasnip, P. J.; W Holzwarth, N. A.; Iuan, D.; Jochym, D. B.; Jollet, F.; Jones, D.; Kresse, G.; Koepernik, K.; Küçükbenli, E.; Kvashnin, Y. O.; M Locht, I. L.; Lubeck, S.; Marsman, M.; Marzari, N.; Nitzsche, U.; Nordström, L.; Ozaki, T.; Paulatto, L.; Pickard, C. J.; Poelmans, W.; Probert, M. I. J.; Refson, K.; Richter, M.; Rignanese, G.-M.; Saha, S.; Scheffler, M.; Schlipf, M.; Schwarz, K.; Sharma, S.; Tavazza, F.; Thunström, P.; Tkatchenko, A.; Torrent, M.; Vanderbilt, D.; van Setten, M. J.; Van Speybroeck, V.; Wills, J. M.; Yates, J. R.; Zhang, G.-X.; Cottenier, S. Reproducibility in density functional theory calculations of solids. *Science* **2016**, *351*, 1415.
(127) Willand, A.; Kvashnin, Y. O.; Genovese, L.; Vázquez-Mayogoitia, A.; Deb, A. K.; Sadeghi, A.; Detustch, T.; Goedecker, S. Norm-conserving pseudopotentials with chemical accuracy compared to all-electron calculations. *J. Chem. Phys.* **2013**, *138*, 104109.
(128) Sim, E.; Song, S.; Burke, K. Quantifying density errors in DFT. *J. Phys. Chem. Lett.* **2018**, *9*, 6385−6392.
(129) Vuckovic, S.; Song, S.; Kozlowski, J.; Sim, E.; Burke, K. Density functional analysis: The theory of density-corrected DFT. *J. Chem. Theory Comput.* **2019**, *15*, 6636−6646.
(130) Santra, G.; Martin, J. M. What types of chemical problems benefit from density-corrected DFT? A probe using an extensive and chemically diverse test suite. *J. Chem. Theory Comput.* **2021**, *17*, 1368−1379.

https://doi.org/10.1021/acs.jctc.3c00089
J. Chem. Theory Comput. 2023, 19, 2827−2841